

Minimal Entanglement and Emergent Symmetries in Low-energy QCD

Qiaofeng Liu^{a,b}, Ian Low^{b,c} and Thomas Mehen^a

^a*Department of Physics, Duke University, Durham, NC 27708, USA*

^b*Department of Physics and Astronomy, Northwestern University, Evanston, IL 60208, USA*

^c*High Energy Physics Division, Argonne National Laboratory, Argonne, IL 60439, USA*

Abstract

We study low-energy scattering of spin- $\frac{1}{2}$ baryons from the perspective of quantum information science, focusing on the correlation between entanglement minimization and the appearance of accidental symmetries. The baryon transforms as an octet under the $SU(3)$ flavor symmetry and its interactions below the pion threshold are described by contact operators in an effective field theory (EFT) of QCD. Despite there being 64 channels in the 2-to-2 scattering, only six independent operators in the EFT are predicted by $SU(3)$. We show that successive entanglement minimization in $SU(3)$ -symmetric channels are correlated with increasingly large emergent symmetries in the EFT. In particular, we identify scattering channels whose entanglement suppression are indicative of emergent $SU(6)$, $SO(8)$, $SU(8)$, and $SU(16)$ symmetries. We also observe the appearance of non-relativistic conformal invariance in channels with unnaturally large scattering lengths. Improved precision from lattice simulations could help determine the degree of entanglement suppression, and consequently the amount of accidental symmetry, in low-energy QCD.

CONTENTS

I. Introduction	2
II. Entanglement and Entanglement Power	5
III. Natural and Unnatural Scattering Lengths	8
IV. EFT for Nucleons and Baryons	10
V. S -matrices in Baryon-baryon scattering	15
A. Flavors in np scattering	15
B. Baryon-baryon scattering	17
C. Minimally entangling S -matrix	21
VI. Entanglement Minimum and Symmetry	24
A. Minimal entanglement in 1-dim sectors – $SU(6)$	26
B. Minimal entanglement in 3-dim sectors – $SO(8)$	27
C. Minimal entanglement in 6-dim sector – $SU(8)$ and $SU(16)$	29
VII. Results from Lattice QCD	30
VIII. Conclusion	31
Acknowledgments	32
A. Pionless EFT for nucleons and baryons	32
B. Baryon-baryon scattering channels	35
References	41

I. INTRODUCTION

Symmetry is among the most fundamental concepts underlying all branches of physics. It is the most powerful guiding principle in formulating laws of nature. Traditionally, there are two views on how symmetry enters into a physical system: those emergent from long-range

fluctuations at long distances and those taken as fundamental at very high energy or short distances. The first viewpoint is exemplified in the appearance of scale invariance during a second-order phase transition while the second is embodied in the fact that all known fundamental interactions in nature are dictated by symmetry principles. However, for such a pillar of modern physics there have been very few studies on where the symmetry comes from. Can symmetry be derived from even more fundamental principles?

In pondering the origin of symmetry, a promising line of thought stems from applying tools in quantum information, in particular the concept of entanglement, to study systems with accidental, emergent symmetries in the infrared [1, 2]. The system of interest is low-energy scattering of nucleons (protons and neutrons) which exhibit accidental approximate symmetries not transparent in the fundamental QCD Lagrangian. They include Wigner’s supermultiplet $SU(4)_{sm}$ [3, 4], where the two spin states of protons and neutrons combine into a fundamental representation of $SU(4)_{sm}$, as well as the Schrödinger invariance which is the non-relativistic conformal group and the largest symmetry group preserving the Schrödinger equation [5]. In addition, simulations from lattice QCD suggest that, for spin- $\frac{1}{2}$ baryons transforming as the octet of $SU(3)$ flavor symmetry,¹ there could be an emergent $SU(16)_{sm}$ symmetry analogous to Wigner’s $SU(4)_{sm}$, where the two spin states of the eight baryons furnish a 16-dimensional fundamental representation of $SU(16)_{sm}$ [6].² Reference [1] made the fascinating observation that the regions of parameter space where the accidental symmetries emerge coincide with regions where the spin entanglement in the 2-to-2 scattering of a proton and a neutron is suppressed, while Ref. [2] studied the observation in a quantum information-theoretic setting and showed that the S -matrix in the spin space, when viewed as a quantum logic gate, corresponds to an Identity gate in the case of $SU(4)_{sm}$ and $SU(16)_{sm}$ and a SWAP gate in the case of Schrödinger symmetry.³

These initial findings hint at a rich interplay between entanglement and symmetry and suggest a potentially fruitful probe for the emergence of accidental symmetries using quan-

¹ The $SU(3)$ flavor symmetry acts on the u -, d - and s -quark, which together transform as the fundamental representation of $SU(3)$. It is an exact symmetry of the QCD Lagrangian when the quark masses are neglected, which is a good approximation for (u, d, s) quarks. Spin- $\frac{1}{2}$ octet baryons are three-quark bound states of (u, d, s) .

² Although Wigner’s $SU(4)_{sm}$ can be seen as a consequence of large N_c expansion [7], no similar explanation exists for $SU(16)_{sm}$.

³ An Identity gate preserves the spin of qubits (nucleons) while a SWAP gate interchanges the spin of the two qubits. Moreover, these are the only two minimal entanglers for a two-qubit system [2].

tum information science. In this work we extend the analyses of Refs. [1, 2] on neutrons (n) and protons (p) to the eight spin- $\frac{1}{2}$ baryons transforming as an octet under the $SU(3)$ flavor symmetry: $\{n, p, \Sigma^+, \Sigma^0, \Sigma^-, \Xi^-, \Xi^0, \Lambda\}$. As we will see, because of the rich theoretical structure, the octet baryon offers a fertile playground to further explore the correlation between entanglement minimization and emergent symmetries. Moreover, unlike the scattering of a neutron and a proton, the scattering of two baryons in general can change flavors and the outgoing particles do not have to be the same as the incoming particles. For example, n and Λ have a non-zero probability of scattering into p and Σ^- . This feature together with the Pauli exclusion principle, which forces the total wave function of the two incoming/outgoing fermions to be totally antisymmetric, create a subtle interplay between flavor and spin quantum numbers that is not present in the np scattering.

We will focus on the very-low-energy scattering of spin- $\frac{1}{2}$ baryons, below the energy threshold for pion production. In this case the process is described by an EFT of QCD using only contact interactions and the leading order Lagrangian contains only six independent operators [8]. The number six is predicted by $SU(3)$ group theory because the product of two octets contains six irreducible representations (irrep): $\mathbf{8} \times \mathbf{8} = \mathbf{27} \oplus \mathbf{10} \oplus \overline{\mathbf{10}} \oplus \mathbf{8}_S \oplus \mathbf{8}_A \oplus \mathbf{1}$. Moreover, since the electric charge and the strangeness quantum number are both conserved in strong interactions, we classify the initial states according to the total electric charge Q and the strangeness S , which must remain the same throughout the scattering process. Our analysis uncovers an intriguing pattern that, successive entanglement minimization in $SU(3)$ -symmetric and Q/S -preserving channels is achieved, an increasingly larger symmetry group appears in the low-energy EFT. We will identify the scattering channels whose spin-entanglement need to be minimized in order to obtain $SU(6)$ spin-flavor symmetries, $SO(8)$ and $SU(8)$ flavor symmetries, as well as $SU(16)_{em}$ spin-flavor symmetry. In addition, in the case of unnatural scattering length, entanglement suppression leads to non-relativistic conformal symmetry in some scattering channels, similar to the np scattering.⁴ Our findings call for improved precision in lattice QCD simulations of baryon-baryon interactions in the case of natural scattering length, in order to determine the amount of emergent symmetry in low-energy QCD.

This paper is organized as follows. In Sec. II we review measures of entanglement and the

⁴ There are other intriguing works on entanglement suppression in scattering of diverse objects, ranging from black holes [9, 10] to pions [11].

definition of entanglement power of operators. We will be applying this measure to find the minimally entangling baryon S -matrices. In Sec. III we discuss the momentum expansion of the S -matrix for the cases of natural and unnatural scattering length. Succinctly, when the scattering length is natural, i.e., of order the range of the forces, the S -matrix is expanded in a power series in the momentum. When the scattering length is unnaturally large the momentum expansion is modified so that powers of the momentum times scattering length are summed to all orders. Effective field theories of baryons for dealing with these two scenarios are described in Sec. IV. In Sec. V, the structure of the baryon-baryon S -matrix is presented. Then minimally entangling S -matrices and their constraints on phase shifts are considered. In Sec. VI the symmetries of the Lagrangian at each entanglement minimum are considered, followed by a comparison with the numerical simulation in lattice QCD in Sec. VII. Our conclusions are given in Sec. VIII. This paper has two appendices. Appendix A gives a review of the pionless EFT for nucleon scattering and Appendix B gives the composition of baryon states for each irrep of $SU(3)$.

II. ENTANGLEMENT AND ENTANGLEMENT POWER

In this section, we briefly review and summarize some of the key concepts in quantum information which are needed in our analysis. We will start with entanglement, which is a property associated with quantum states, and proceed to introduce the entanglement power of an operator.

A quantum state of a system is entangled if it cannot be written as a tensor-product state of its sub-systems. In this case a measurement on a sub-system can modify the state of the rest of the system. Specifically let us consider a bipartite system \mathcal{H}_{12} , such as the two-particle system in scattering, whose Hilbert space can be written as a tensor-product space: $\mathcal{H}_{12} = \mathcal{H}_1 \otimes \mathcal{H}_2$. A state vector $|\psi\rangle \in \mathcal{H}_{12}$ is *entangled* if it is not separable, i.e., there do not exist $|\psi_1\rangle \in \mathcal{H}_1$ and $|\psi_2\rangle \in \mathcal{H}_2$ such that $|\psi\rangle = |\psi_1\rangle \otimes |\psi_2\rangle$.

An entanglement measure is a way to quantify the degree of entanglement of any given state. There are multiple entanglement measures. For a bipartite system, the commonly employed von Neumann entropy is defined as

$$E(\rho) = -\text{Tr}(\rho_1 \ln \rho_1) = -\text{Tr}(\rho_2 \ln \rho_2) , \quad (1)$$

where $\rho = |\psi\rangle\langle\psi|$ is the density matrix and $\rho_{1(2)} = \text{Tr}_{2(1)}(\rho)$ is the reduced density matrix obtained after tracing over subsystem 2(1). In computations it is often more convenient to calculate the linear entropy

$$E(\rho) = -\text{Tr}(\rho_1(\rho_1 - 1)) = 1 - \text{Tr}\rho_1^2, \quad (2)$$

which has the advantage of being a polynomial of ρ_1 . The entanglement measures have the property that they reach zero on a product state $|\psi_A\rangle \otimes |\psi_B\rangle$ and attain a maximum on a maximally entangled state

For a system with two spin- $\frac{1}{2}$ particles, one often defines the ‘‘computational basis’’ as $\{|\uparrow\uparrow\rangle, |\uparrow\downarrow\rangle, |\downarrow\uparrow\rangle, |\downarrow\downarrow\rangle\}$, where $|ij\rangle = |i\rangle_1 \otimes |j\rangle_2$ and an up (down) arrow represents the eigenstate of σ_z with eigenvalues $+1$ (-1). Then for a general normalized spin state

$$|\psi\rangle = \alpha |\uparrow\uparrow\rangle + \beta |\uparrow\downarrow\rangle + \gamma |\downarrow\uparrow\rangle + \delta |\downarrow\downarrow\rangle, \quad |\alpha|^2 + |\beta|^2 + |\gamma|^2 + |\delta|^2 = 1, \quad (3)$$

its entanglement can be calculated using the linear entropy in Eq. (2). The reduced density matrix ρ_1 for the first spin is

$$\rho_1 = \text{Tr}_2 |\psi\rangle\langle\psi| = \begin{pmatrix} |\alpha|^2 + |\beta|^2 & \alpha\gamma^* + \beta\delta^* \\ \alpha^*\gamma + \beta^*\delta & |\gamma|^2 + |\delta|^2 \end{pmatrix}, \quad (4)$$

and the entanglement of $|\psi\rangle$ is therefore

$$E(|\psi\rangle) = 1 - \text{Tr}_1\rho_1^2 = 2|\alpha\delta - \beta\gamma|^2. \quad (5)$$

It is easy to show that (i) if $|\psi\rangle = (a|\uparrow\rangle_1 + b|\downarrow\rangle_1) \otimes (c|\uparrow\rangle_2 + d|\downarrow\rangle_2)$ is a product state, $E(|\psi\rangle) = 0$, and (ii) the maximal entanglement is $1/2$, which is the case for the maximally entangled Bell states $(|\uparrow\uparrow\rangle \pm |\downarrow\downarrow\rangle)/\sqrt{2}$ and $(|\uparrow\downarrow\rangle \pm |\downarrow\uparrow\rangle)/\sqrt{2}$.

The linear entropy is related to another measure of spin entanglement, the concurrence $\Delta = |\alpha\delta - \beta\gamma|$ introduced in Ref. [12]. Both measures have the range $(0, 1/2)$. In fact, it is possible to show that every entanglement measure for the bipartite qubit system can be expressed in terms of the concurrence Δ [2].

The entanglement measure quantifies the entanglement in a quantum state $|\psi\rangle$, while the

entanglement power measures the ability of a quantum-mechanical operator U to generate entanglement by averaging over all direct product states it acts on [13, 14]:

$$E(U) = \overline{E(U |\psi_1\rangle \otimes |\psi_2\rangle)} , \quad (6)$$

where the average is over the state space \mathcal{H}_1 and \mathcal{H}_2 . For qubits we simply average over each Bloch sphere or, equivalently, integrate over all rotations.

There is, however, a subtlety in the definition of the entanglement power. It is clear that an operator that is local in the product space, $U_1 \otimes U_2$, should leave the entanglement of the initial state unchanged, where $U_{1/2}$ is a single-qubit operator acting on $\mathcal{H}_{1/2}$. This leads to the notion of equivalent classes,

$$U \sim U' \quad \text{if} \quad U = (U_1 \otimes U_2)U'(V_1 \otimes V_2) . \quad (7)$$

Modulo the redundancy in each equivalent class, it was shown in Ref. [2] that, for a two-qubit system where $U \in SU(4)$, there are only two operators which minimize the entanglement power in Eq. (6): the Identity and the SWAP. They have the following matrix representations in the computational basis,

$$\mathbf{1} = \begin{pmatrix} 1 & 0 & 0 & 0 \\ 0 & 1 & 0 & 0 \\ 0 & 0 & 1 & 0 \\ 0 & 0 & 0 & 1 \end{pmatrix}, \quad \text{SWAP} = \begin{pmatrix} 1 & 0 & 0 & 0 \\ 0 & 0 & 1 & 0 \\ 0 & 1 & 0 & 0 \\ 0 & 0 & 0 & 1 \end{pmatrix} . \quad (8)$$

SWAP interchanges the states of two qubits, which makes it clear that it has minimal entanglement power. It is useful to write SWAP in the product space using Pauli matrices,

$$\text{SWAP} = (1 + \boldsymbol{\sigma} \cdot \boldsymbol{\sigma})/2 , \quad \boldsymbol{\sigma} \cdot \boldsymbol{\sigma} \equiv \sum_a \boldsymbol{\sigma}^a \otimes \boldsymbol{\sigma}^a . \quad (9)$$

In this paper, we primarily study the very low-energy scattering of nucleons and other spin-1/2 baryons, which is dominated by the s -wave for non-identical particles. This implies

that the S -matrix for np scattering can be written as [2]

$$S = \frac{1}{2} (e^{2i\delta_1} + e^{2i\delta_0}) 1 + \frac{1}{2} (e^{2i\delta_1} - e^{2i\delta_0}) \text{ SWAP} , \quad (10)$$

where δ_0 and δ_1 are the scattering phases in the spin singlet and triplet channels, respectively. In general these phases could depend on the center-of-mass momentum p . One can see that $S \propto 1$ if $\delta_0 = \delta_1$ and $S \propto \text{SWAP}$ if $|\delta_0 - \delta_1| = \pi/2$. They correspond to the $SU(4)_{sm}$ spin-flavor symmetry and the Schrödinger symmetry, respectively. Note that $p \cot \delta_i(p) = -1/a_i + r_{0i} p^2/2 + \dots$, so $\delta_0 = \delta_1$ can be arranged by imposing a symmetry that makes the scattering parameters in the two channels equal. Imposing $|\delta_0 - \delta_1| = \pi/2$ for all p is difficult since the $\delta_i(p)$ are complicated functions of p so if the constraint is enforced at one value of momentum it will generically not hold at other values of momentum. However, there is an exception when $\delta_0 = 0$ and $\delta_1 = \pm\pi/2$ (or vice versa) for all p . $\delta_0 = 0$ corresponds to $a_0 = 0$; this is a free theory and the S -matrix is trivial. $\delta_1 = \pm\pi/2$ corresponds to $1/a_1 = 0$, $r_{1i} = 0$; this corresponds to the unitarity limit [5]. Both the free theory and the theory at the unitarity limit are invariant under the Schrödinger symmetry, so this is how $|\delta_0 - \delta_1| = \pi/2$ can be realized in a natural way [2].

We will derive the generalization of Eq. (10) for octet baryons, which allows us to directly recognize when the S -matrix is minimally entangling, thereby sidestepping the procedure of averaging over initial product states in the definition of entanglement power in Eq. (6). This simplifies our analysis greatly.

III. NATURAL AND UNNATURAL SCATTERING LENGTHS

In this section we introduce the concept of natural and unnatural scattering lengths in the scattering of non-relativistic particles, focusing on the s -wave channel. Assuming a single channel, an equal mass M , and energy below any inelastic threshold, the S -matrix for spinless non-relativistic particles can be written as

$$S = e^{2i\delta(p)} = 1 + i \frac{Mp}{2\pi} \mathcal{A} , \quad (11)$$

where p is the center-of-mass momentum, $\delta(p)$ is the phase shift and \mathcal{A} is the scattering amplitude. Rewriting $e^{2i\delta} = (1 + i \tan \delta)/(1 - i \tan \delta)$ allows us to express

$$\mathcal{A} = \frac{4\pi}{M} \frac{1}{p \cot \delta - ip}. \quad (12)$$

It has been long known that $p \cot \delta$ admits an expansion in p^2/Λ^2 , where Λ is determined by the range of the two-body potential such that it dies off exponentially when the distance r satisfies $r\Lambda > 1$ [15]:

$$p \cot \delta = -\frac{1}{a} + \frac{1}{2} r_0 p^2 + \dots = -\frac{1}{a} + \frac{1}{2} \Lambda^2 \sum_{n=0}^{\infty} r_n \left(\frac{p^2}{\Lambda^2} \right)^n. \quad (13)$$

In the above a is the scattering length, r_0 is the effective range, r_1 is the shape parameter, etc. These parameters are measured experimentally. In particular, a characterizes the effective size of the target and is related to the total cross-section $\sigma_{tot} \rightarrow 4\pi a^2$ as $p \rightarrow 0$. Equation (13) is referred to as the effective range expansion (ERE) [16].

The S -matrix of a free theory is $S = 1$ and $\tan \delta = 0$ ($\delta = 0$); the scattering length a and all r_i 's vanish. On the other hand, the interaction is “maximal” when $S = -1$ and $\tan \delta = \infty$ ($\delta = \pi/2$); in this case $a \rightarrow \infty$ with all other parameters in Eq. (13) vanishing and the cross-section is $\sigma_{tot} = 4\pi/p^2$, which satisfies the unitarity bound. This is the theory with the largest possible cross section consistent with unitarity and hence this is known as the “unitarity limit.” Moreover, at both $\delta = 0$ and $\delta = \pi/2$ the theory exhibits Schrödinger symmetry, which is sometimes referred to as non-relativistic conformal invariance, since there is no length scale [5].

In a generic finite-range potential the parameters r_i 's in Eq. (13) are expected to be of $\mathcal{O}(1/\Lambda)$ for all i . However a can take any value: it is positive for an attractive potential with bound states, goes to infinity when the bound state is at threshold and has zero binding energy, and becomes negative for weakly attractive potential with resonances (virtual bound states). Recall that bound states are poles in the S -matrix residing on the positive imaginary axis on the complex plane and have normalizable wave functions. Resonances are poles in the lower half complex plane whose wave functions are non-normalizable.

When the scattering length is large compared to $1/\Lambda$, it introduces a subtlety in the perturbative expansion of \mathcal{A} in p/Λ . Applying the ERE in Eq. (13) to \mathcal{A} in Eq. (12), there

are two scenarios we would like to highlight:

- (i) Natural scattering length: this is when $|a| \lesssim 1/\Lambda$ (and $|r_i| \lesssim 1/\Lambda$.) In this case the expansion of \mathcal{A} in powers of momentum converges up to $p \sim \Lambda$:

$$\begin{aligned} \mathcal{A} &= -\frac{4\pi a}{M} \left[1 - iap + \left(\frac{1}{2} ar_0 - a^2 \right) p^2 + O(p^3/\Lambda^3) \right] \\ &= \sum_{n=0}^{\infty} \mathcal{A}_n, \quad \text{where} \quad \mathcal{A}_n \sim \mathcal{O}(p^n). \end{aligned} \quad (14)$$

The leading order (LO) contribution is $\mathcal{A}_0 \sim \mathcal{O}(p^0)$.

- (ii) Unnatural scattering length: $|a| \gg 1/\Lambda$, in which case the expansion breaks down when $p \sim 1/|a|$, far below Λ . It is then necessary to keep ap to all orders when expanding in p/Λ [17, 18],

$$\begin{aligned} \mathcal{A} &= -\frac{4\pi}{M} \frac{1}{(1/a + ip)} \left[1 + \frac{r_0/2}{(1/a + ip)} p^2 + \frac{(r_0/2)^2}{(1/a + ip)^2} p^4 + \dots \right] \\ &= \mathcal{A}_{-1} + \sum_{n=0}^{\infty} \mathcal{A}_n, \quad \text{where} \quad \mathcal{A}_n \sim \mathcal{O}(p^n). \end{aligned} \quad (15)$$

Notice that the LO term in the amplitude now scales with p^{-1} for $p > 1/|a|$.

In low-energy nucleon-nucleon scattering, there is a bound state, the deuteron, in the spin-triplet channel (3S_1) with the scattering length $a_1 \approx 5.4$ fm, and a near-threshold virtual bound state in the spin-singlet channel (1S_0) with $a_0 \approx -23.7$ fm. These are (much) larger than the Compton wavelength of pions, $1/m_\pi \approx 1.4$ fm, which sets the range of nuclear interactions. The fact that the two-nucleon system has scattering lengths (much) larger than $1/m_\pi$ is the reason why it is often stated that nuclear physics is finely-tuned or unnatural [19].

IV. EFT FOR NUCLEONS AND BARYONS

In the seminal papers [20, 21] Weinberg proposed using the EFT framework to describe nucleon-nucleon interactions, which has the advantage of employing a systematic expansion with well-defined error estimates for the computation of any observables. Moreover, for the purpose of this work it is worth emphasizing that the EFT Lagrangian makes the presence of

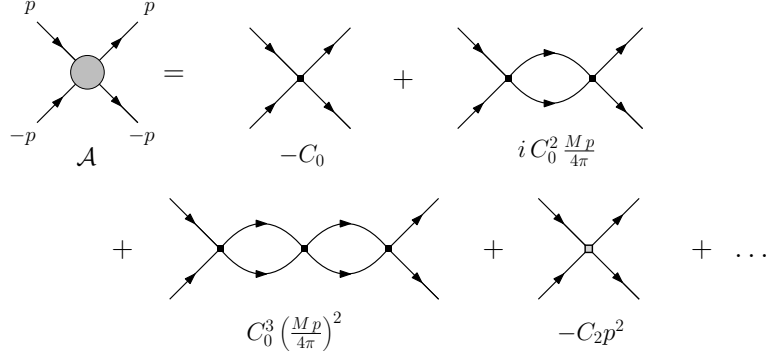


FIG. 1. The first few diagrams contributing to the s -wave amplitude in the center-of-mass frame. A solid black vertex represents the $-C_0$ vertex, and a grey vertex represents the $-C_2 p^2$ vertex.

(approximate) symmetries transparent. Traditionally the EFT technique requires a separation of scales in the physical system of interest, which in the two-nucleon case is complicated by the presence of unnaturally large scattering lengths.

We start by considering the effective Lagrangian for a non-relativistic fermion ψ that is invariant under Galilean, parity, and time-reversal symmetries [17, 18]:

$$\mathcal{L}_{eff} = \psi^\dagger \left(i\partial_t + \frac{\nabla^2}{2M} \right) \psi + C_0 (\psi^\dagger \psi)^2 + \frac{C_2}{8} \left[(\psi\psi)^\dagger (\psi \overleftrightarrow{\nabla}^2 \psi) + \text{h.c.} \right] + \dots, \quad (16)$$

where

$$\overleftrightarrow{\nabla}^2 \equiv \overleftarrow{\nabla}^2 - 2\overleftarrow{\nabla} \cdot \overrightarrow{\nabla} + \overrightarrow{\nabla}^2, \quad (17)$$

is dictated by the Galilean invariance. Terms omitted in \mathcal{L}_{eff} are contact operators containing more derivatives and/or more fields. In particular, C_{2n} are couplings of contact operators with $2n$ spatial gradients.⁵ We will focus on the s -wave channel and assume the mass M is very large so that relativistic corrections can be neglected. Equation (16) can be employed to describe two-nucleon interactions below the pion threshold. In this ‘‘Pionless EFT’’ pions are integrated out and the EFT is expected to be valid for $p \lesssim \Lambda \sim m_\pi$, where $p = \sqrt{ME}$ and E is the momentum and total energy in the center-of-mass frame, respectively.

In the EFT the amplitude \mathcal{A} is usually computed by summing a series of Feynman diagrams to the desired order in the p/Λ expansion. This is illustrated in Fig. 1: at $\mathcal{O}(p^0)$, \mathcal{A}_0 comes from a single tree-diagram with one C_0 vertex, while \mathcal{A}_1 arises from a one-loop

⁵ Time derivatives beyond the kinetic term are eliminated in favor of spatial derivatives.

diagram with two insertions of C_0 . Going up to $\mathcal{O}(p^2)$, there are two diagrams, a two-loop diagram with three insertions of C_0 and a tree-diagram with one factor of C_2 , contributing to \mathcal{A}_2 . Notice that, in non-relativistic EFT, particles and anti-particles are conserved separately and the only loop-diagrams are the bubble diagrams shown in Fig. 1. Importantly, the loop integrals are UV-divergent and a subtraction scheme is required to remove the UV divergences. In what follows we summarize the results and relegate the technical details to Appendix A.

The goal is to have an expansion of the amplitude calculated from EFT that matches ERE. This matching allows us to relate the EFT parameters to physical scattering parameters. Since natural and unnatural scattering have different amplitude expansions, one would also expect different expansion parameters in EFT. This is achieved by carefully selecting the subtraction scheme and the way bubble diagrams are resummed.

The commonly used minimal subtraction (MS) scheme will match the ERE in the natural case. One finds that

$$C_0 = \frac{4\pi a}{M}, \quad C_2 = C_0 \frac{a r_0}{2}. \quad (18)$$

In general, when the scattering length is of the natural size $a \sim \mathcal{O}(1/\Lambda)$, $C_{2n} \sim 4\pi/(M\Lambda^{2n+1})$. But when a is anomalously large, we find instead $C_{2n} \sim 4\pi a^{n+1}/(M\Lambda^n)$ and the perturbative expansion in p/Λ breaks down when $1/a \lesssim p \ll \Lambda$. This is evident in Eq. (15), where the expansion of \mathcal{A} in ERE starts at $\mathcal{A}_{-1} \sim 1/p$ for $1/a \lesssim p$.

It is clear that \mathcal{A}_{-1} , involving a negative power in p , can only come from summing over an infinite set of diagrams in perturbation. Moreover, a small coupling must exist to justify the resummation. This is achieved by choosing a different subtraction scheme, the power divergence subtraction (PDS), introduced in Refs. [17, 18], which subtracts both the $1/(D-3)$ and the $1/(D-4)$ poles in the bubble diagram. The PDS subtraction introduces a renormalization scale dependence in the Wilson coefficients $C_{2n} = C_{2n}(\mu)$ and \mathcal{A}_{-1} arises from summing an infinite number of bubble diagrams with only C_0 insertions. In the end,

$$C_0(\mu) = \frac{4\pi}{M} \left(\frac{1}{-\mu + 1/a} \right), \quad C_2(\mu) = \frac{4\pi}{M} \left(\frac{1}{-\mu + 1/a} \right)^2 \frac{r_0}{2}. \quad (19)$$

The μ dependence makes it possible to establish a new power counting, the KSW-vK counting [17, 18, 22], which allows for convergence of perturbative expansion over a much larger

range of momentum when the scattering length is unnaturally large. This can be seen by taking $\mu \ll 1/|a|$, then $C_{2n}(\mu) \sim (4\pi/M\Lambda^n)(1/\mu^{n+1})$. Therefore, when $1/|a| \ll p \lesssim \Lambda$, we choose $\mu \sim p$ and

$$C_{2n} p^{2n} \sim p^{n-1} . \quad (20)$$

So formally $C_0 \sim 1/p$, whose insertions need to be resummed to all orders while insertions of all other $C_{2n>0}$ carry positive powers of p and can be treated perturbatively.

For neutrons and protons, their masses are almost identical and the EFT has an $SU(2)_I$ isospin symmetry under which they transform as a fundamental representation. Introducing p and n as two-component Pauli spinors representing the two spin states of the proton and neutron, respectively, the LO interactions in the EFT can be written as [4]

$$\mathcal{L}_{\text{LO}}^{n_f=2} = -\frac{1}{2}C_S (N^\dagger N)^2 - \frac{1}{2}C_T (N^\dagger \boldsymbol{\sigma} N) \cdot (N^\dagger \boldsymbol{\sigma} N) , \quad N = \begin{pmatrix} p \\ n \end{pmatrix} , \quad (21)$$

where the Pauli matrices $\boldsymbol{\sigma} = (\sigma^1, \sigma^2, \sigma^3)$ only acts on the spin degrees of freedom. C_S and C_T can be expressed in terms of the couplings in the 1S_0 and 3S_1 channels as $\bar{C}_0 = C_S - 3C_T$ and $\bar{C}_1 = C_S + C_T$, respectively, where $\bar{C}_i = (4\pi/M)[1/(-\mu + 1/a_i)]$, $i = 0, 1$, as in Eq. (19). M is now the nucleon mass and a_0 (a_1) is the nucleon-nucleon scattering length in the 1S_0 (3S_1) channel. Observe that, when $C_T = 0$, we have $\bar{C}_0 = \bar{C}_1$ which is an indication of Wigner's $SU(4)_{sm}$ spin-isospin symmetry [3, 4], under which N transforms as a fundamental representation of $SU(4)_{sm}$ and the C_S operator is invariant. On the other hand, $a_i \rightarrow \pm\infty$ is a non-trivial fixed point since $\mu(d/d\mu)[\mu\bar{C}_i(\mu)] = 0$. In addition to $SU(4)$ symmetry [4] in this case one also has the Schrödinger symmetry [5]. Ref. [1] pointed out that both cases of emergent symmetries coincide with regions of parameter where the spin-entanglement is suppressed in the 2-to-2 scattering of nucleons. Moreover, the S -matrix as a quantum logic gate is the Identity for $SU(4)_{sm}$ and the SWAP for Schrödinger symmetry [2].

In low-energy QCD the nucleons are part of the spin-1/2 baryons which transform as an octet under the $SU(3)$ flavor symmetry acting on the light flavor quarks: (u, d, s) . The EFT consistent with the $SU(3)_L \times SU(3)_R$ chiral symmetry of QCD is expressed in terms of the

3×3 octet matrix B :

$$B = \begin{pmatrix} \Sigma^0/\sqrt{2} + \Lambda/\sqrt{6} & \Sigma^+ & p \\ \Sigma^- & -\Sigma^0/\sqrt{2} + \Lambda/\sqrt{6} & n \\ \Xi^- & \Xi^0 & -\sqrt{\frac{2}{3}}\Lambda \end{pmatrix} \quad (22)$$

It is worth pointing out that, in contrast to the similar matrix for the meson octet, the baryon matrix B is not Hermitian because charge conjugation does not return to the same states; instead it changes baryons to antibaryons. The LO effective Lagrangian contains six contact operators [8]:

$$\begin{aligned} \mathcal{L}_{\text{LO}}^{n_f=3} = & -c_1 \langle B_i^\dagger B_i B_j^\dagger B_j \rangle - c_2 \langle B_i^\dagger B_j B_j^\dagger B_i \rangle - c_3 \langle B_i^\dagger B_j^\dagger B_i B_j \rangle - c_4 \langle B_i^\dagger B_j^\dagger B_j B_i \rangle \\ & - c_5 \langle B_i^\dagger B_i \rangle \langle B_j^\dagger B_j \rangle - c_6 \langle B_i^\dagger B_j \rangle \langle B_j^\dagger B_i \rangle, \end{aligned} \quad (23)$$

where $\langle \dots \rangle$ denotes the trace over the matrices and $i = 1, 2$ denotes the two spin states of the baryon. Repeated spin indices are summed over implicitly. It is important to point out that there is a double-trace operator, $\langle B_i^\dagger B_j^\dagger \rangle \langle B_i B_j \rangle$, which in the literature is eliminated using the Cayley-Hamilton identity [8]:

$$\begin{aligned} & \frac{1}{2} \langle B_i^\dagger B_i B_j^\dagger B_j \rangle - \frac{1}{2} \langle B_i^\dagger B_j B_j^\dagger B_i \rangle - \langle B_i^\dagger B_j^\dagger B_i B_j \rangle + \langle B_i^\dagger B_j^\dagger B_j B_i \rangle \\ = & \frac{1}{2} \langle B_i^\dagger B_i \rangle \langle B_j^\dagger B_j \rangle - \frac{1}{2} \langle B_i^\dagger B_j \rangle \langle B_j^\dagger B_i \rangle - \frac{1}{2} \langle B_i^\dagger B_j^\dagger \rangle \langle B_i B_j \rangle. \end{aligned} \quad (24)$$

The fact that there are only six operators at LO is a consequence of $SU(3)$ flavor symmetry group, which will be discussed in the next section.

It is worth mentioning that in the large N_c limit, when the number of color $N_c \rightarrow \infty$, the $SU(3)$ flavor symmetry at the quark level is enlarged into the $SU(6)$ quark spin-flavor symmetry [7], under which the spin indexes of the u , d , and s quarks, together with the flavor quantum numbers, combine to transform together as a fundamental representation of $SU(6)$. In this case the spin-1/2 and spin-3/2 baryons combine to form a 56-dimensional representation described by a completely symmetric three-index field $\Psi^{\mu\nu\rho}$. The EFT Lagrangian to

the lowest order contains only two operators [7]:

$$\mathcal{L}_{int} = \left[a (\Psi_{\mu\nu\rho}^\dagger \Psi^{\mu\nu\rho})^2 + b \Psi_{\mu\nu\sigma}^\dagger \Psi^{\mu\nu\tau} \Psi_{\rho\delta\tau}^\dagger \Psi^{\rho\delta\sigma} \right]. \quad (25)$$

In this limit of $SU(6)$ spin-flavor symmetry, the six Wilson coefficients in Eq. (23) are related to a and b in the above [7]:

$$c_1 = -\frac{7}{27}b, \quad c_2 = \frac{1}{9}b, \quad (26)$$

$$c_3 = \frac{10}{81}b, \quad c_4 = -\frac{14}{81}b, \quad (27)$$

$$c_5 = a + \frac{2}{9}b, \quad c_6 = -\frac{1}{9}b. \quad (28)$$

We will work out the quantum information-theoretic prediction of the $SU(6)$ symmetry.

V. S-MATRICES IN BARYON-BARYON SCATTERING

In this section we study the general S -matrix in baryon-baryon scattering, focusing on the interplay between spin and flavor quantum numbers due to the Fermi-Dirac statistics. We establish our notation and formalism by reconsidering the nucleon-nucleon channel and generalize to octet baryons. Then we derive conditions for the S -matrix to be minimally entangling.

A. Flavors in np scattering

The S -matrix for np scattering in the low-energy limit is dominated by the s -wave and contains two channels, 1S_0 and 3S_1 , and therefore two scattering phases δ_0 and δ_1 . In the two-qubit computational basis, $\{|00\rangle, |01\rangle, |10\rangle, |11\rangle\}$, the S -matrix can be written as

$$S = \frac{1 - \boldsymbol{\sigma} \cdot \boldsymbol{\sigma}}{4} e^{2i\delta_0} + \frac{3 + \boldsymbol{\sigma} \cdot \boldsymbol{\sigma}}{4} e^{2i\delta_1} \quad (29)$$

where $(1 - \boldsymbol{\sigma} \cdot \boldsymbol{\sigma})/4$ and $(3 + \boldsymbol{\sigma} \cdot \boldsymbol{\sigma})/4$ project onto spin states in the 1S_0 and 3S_1 subspaces, respectively. The S -matrix is manifestly unitary, $SS^\dagger = 1$. It will be convenient to rewrite

Eq. (29) in terms of the Identity and SWAP operators defined in Eq. (9) [2],

$$S = \frac{1 - \text{SWAP}}{2} e^{2i\delta_0} + \frac{1 + \text{SWAP}}{2} e^{2i\delta_1} = 1 (e^{2i\delta_0} + e^{2i\delta_1}) + \text{SWAP} (e^{2i\delta_1} - e^{2i\delta_0}) , \quad (30)$$

from which we see the S -matrix is proportional to an Identity gate when $\delta_0 = \delta_1$ and the SWAP gate when $|\delta_0 - \delta_1| = \pi/2$.

In nature neutrons and protons are almost degenerate in mass, due to the small mass splitting between u - and d -quarks, which leads to the existence of approximate $SU(2)_I$ isospin symmetry. Under $SU(2)_I$ the proton and neutron are particles with identical isospin quantum number $I = 1/2$ but different $I_3 = \pm 1/2$. Using the notation $|I, I_3\rangle$ we have $p = |1/2, 1/2\rangle$ and $n = |1/2, -1/2\rangle$. It is instructive to reconsider the S -matrix of NN scattering taking into account the isospin invariance, which introduces interesting interplay between flavor and spin quantum numbers due to the Pauli exclusion principle.

The S -matrix for the scattering of two-nucleon $N_i(s_i)N_j(s_j) \rightarrow N_k(s_k)N_l(s_l)$, where s_i represents the spin state of N_i , is now of the tensor-product (spin) \otimes (flavor) = (spin₁ \otimes spin₂) \otimes (flavor₁ \otimes flavor₂):

$$S = \frac{1 - \boldsymbol{\sigma} \cdot \boldsymbol{\sigma}}{4} \otimes \frac{3 + \boldsymbol{\tau} \cdot \boldsymbol{\tau}}{4} e^{2i\delta_0} + \frac{3 + \boldsymbol{\sigma} \cdot \boldsymbol{\sigma}}{4} \otimes \frac{1 - \boldsymbol{\tau} \cdot \boldsymbol{\tau}}{4} e^{2i\delta_1} , \quad (31)$$

where $\boldsymbol{\sigma}^a$ and $\boldsymbol{\tau}^a$ are Pauli matrices in the spin- and flavor-subspace, respectively. Moreover, because of the Fermi-Dirac statistics, the total isospin $I = 1$ projects into the spin singlet 1S_0 , while the $I = 0$ projects into triplet 3S_1 .

It is worth noting that the S -matrix in Eq. (31) is block diagonal in the flavor basis $\{|pp\rangle, |pn\rangle, |np\rangle, |nn\rangle\}$,

$$\frac{3 + \boldsymbol{\tau} \cdot \boldsymbol{\tau}}{4} = \begin{pmatrix} 1 & 0 & 0 & 0 \\ 0 & \frac{1}{2} & \frac{1}{2} & 0 \\ 0 & \frac{1}{2} & \frac{1}{2} & 0 \\ 0 & 0 & 0 & 1 \end{pmatrix} , \quad \frac{1 - \boldsymbol{\tau} \cdot \boldsymbol{\tau}}{4} = \begin{pmatrix} 0 & 0 & 0 & 0 \\ 0 & \frac{1}{2} & -\frac{1}{2} & 0 \\ 0 & -\frac{1}{2} & \frac{1}{2} & 0 \\ 0 & 0 & 0 & 0 \end{pmatrix} . \quad (32)$$

This is because the electric charge Q is a conserved quantity and commutes with the S -matrix. So, alternatively, the NN scattering could be analyzed in individual sectors labeled by the total charge Q . For example, focusing on the $Q = +1$ sector which contains

$\{|pn\rangle, |np\rangle\}$, the S -matrix becomes

$$S = \frac{1 - \boldsymbol{\sigma} \cdot \boldsymbol{\sigma}}{4} \otimes \begin{pmatrix} \frac{1}{2} & \frac{1}{2} \\ \frac{1}{2} & \frac{1}{2} \end{pmatrix} e^{2i\delta_0} + \frac{3 + \boldsymbol{\sigma} \cdot \boldsymbol{\sigma}}{4} \otimes \begin{pmatrix} \frac{1}{2} & -\frac{1}{2} \\ -\frac{1}{2} & \frac{1}{2} \end{pmatrix} e^{2i\delta_1}. \quad (33)$$

In fact, the S -matrix in the flavor subspace is diagonalized in the isospin basis $\{(|pn\rangle + |np\rangle)/\sqrt{2}, (|pn\rangle - |np\rangle)/\sqrt{2}\}$,

$$S = \frac{1 - \boldsymbol{\sigma} \cdot \boldsymbol{\sigma}}{4} \otimes \begin{pmatrix} 1 & 0 \\ 0 & 0 \end{pmatrix} e^{2i\delta_0} + \frac{3 + \boldsymbol{\sigma} \cdot \boldsymbol{\sigma}}{4} \otimes \begin{pmatrix} 0 & 0 \\ 0 & 1 \end{pmatrix} e^{2i\delta_1}, \quad (34)$$

where $(|pn\rangle + |np\rangle)/\sqrt{2}$ is in the total isospin $I = 1$ and $(|pn\rangle - |np\rangle)/\sqrt{2}$ in the total isospin $I = 0$. The projection operators in these two different flavor bases are related by

$$\begin{pmatrix} \frac{1}{2} & \frac{1}{2} \\ \frac{1}{2} & \frac{1}{2} \end{pmatrix} = O_N^\dagger \begin{pmatrix} 1 & 0 \\ 0 & 0 \end{pmatrix} O_N, \quad \begin{pmatrix} \frac{1}{2} & -\frac{1}{2} \\ -\frac{1}{2} & \frac{1}{2} \end{pmatrix} = O_N^\dagger \begin{pmatrix} 0 & 0 \\ 0 & 1 \end{pmatrix} O_N, \quad (35)$$

where

$$O_N = \begin{pmatrix} \frac{1}{\sqrt{2}} & \frac{1}{\sqrt{2}} \\ \frac{1}{\sqrt{2}} & -\frac{1}{\sqrt{2}} \end{pmatrix}. \quad (36)$$

We will see that Eqs. (33) and (34) generalize to baryon-baryon scattering where the isospin $SU(2)_I$ is enlarged to the $SU(3)$ flavor symmetry.

B. Baryon-baryon scattering

Among the baryons, np scattering is special because it is flavor diagonal, meaning the incoming and outgoing particles are identical and do not change their flavor quantum numbers. This is not the case, in general, for the scattering of other baryons. In Fig. 2 we show the lowest-lying spin-1/2 baryon octet, with the states plotted according to their isospin (I_3) and strangeness (S) quantum numbers.⁶ The electric charge, also shown in Fig. 2, is $Q = I_3 + (S + 1)/2$ according to the Gell-Mann-Nishima formula. These baryons furnish an octet representation (**8**) under $SU(3)$ flavor group, which then dictates that there are only

⁶ In a slight abuse of notation we use S to represent both the strangeness quantum number and the S -matrix, with the hope that the distinction is clear from the context.

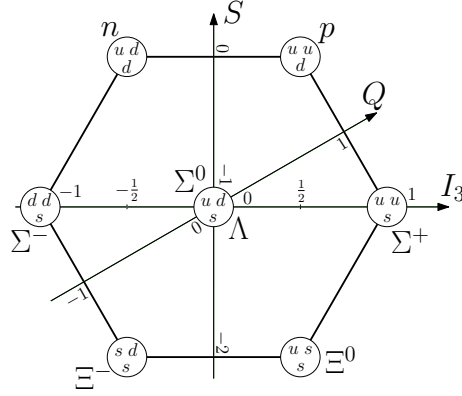


FIG. 2. The spin-1/2 baryons organized in an octet of $SU(3)$ flavor group. The axes, S , Q , and I_3 , represent strangeness, charge, and I_3 , respectively.

six scattering phases in the S -matrix: $\mathbf{8} \otimes \mathbf{8} = \mathbf{27} \oplus \mathbf{10} \oplus \overline{\mathbf{10}} \oplus \mathbf{8}_S \oplus \mathbf{8}_A \oplus \mathbf{1}$, where $\mathbf{27}$, $\mathbf{8}_S$, $\mathbf{1}$ are $SU(3)$ irreducible representations (irreps) symmetric in the flavor quantum numbers and $\mathbf{10}$, $\overline{\mathbf{10}}$, $\mathbf{8}_A$ are antisymmetric. In addition, the Pauli exclusion principle requires that scattering in the $\mathbf{27}$, $\mathbf{8}_S$, $\mathbf{1}$ must be in the 1S_0 channel while $\mathbf{10}$, $\overline{\mathbf{10}}$, $\mathbf{8}_A$ are in 3S_1 . The phases in the S -matrix are labeled as $\delta_{\mathbf{27}}$, $\delta_{\mathbf{8}_S}$, $\delta_{\mathbf{1}}$, $\delta_{\mathbf{10}}$, $\delta_{\overline{\mathbf{10}}}$, $\delta_{\mathbf{8}_A}$.

The presence of flavor non-diagonal channels introduces an additional layer of complexity in the S -matrix and the interplay between flavor and spin quantum numbers have important consequences when it comes to entanglement minimization. When including the flavor quantum number, two comments are in order: (1) in a scattering experiment the $|\text{IN}\rangle$ and $|\text{OUT}\rangle$ states are usually prepared as a pair of particles with definite flavor quantum numbers in Q and S , and (2) in strong interactions Q and S are conserved. Due to these considerations, we classify the initial pair of baryons according to the total Q and S , as shown in Table. I. They are divided into various one-dimensional (1-dim), three-dimensional (3-dim) and six-dimensional (6-dim) sectors and an initial pair in a particular (Q, S) sector is only allowed to scatter into other pairs within the sector. The np channel is flavor-diagonal and resides in the $(Q, S) = (1, 0)$ sector. The S -matrix is block-diagonal in a basis with definite (Q, S) two-baryon states and it is simpler to analyze each sector individually.

We will start with the 1-dim sectors with non-identical particles,⁷ which includes the np channel and involves the $\mathbf{27}$ (flavor symmetric) and the $\mathbf{10}$ or $\overline{\mathbf{10}}$ (flavor antisymmetric)

⁷ For identical particles the particles must be in a spin singlet state and the S -matrix simply multiplies this state by a phase.

	Q	S		Q	S		Q	S
nn	0	0	$\Sigma^-\Sigma^-$	-2	-2	$\Sigma^-\Xi^-$	-2	-3
np	1	0	$\Sigma^-\Lambda$			$\Sigma^-\Xi^0$		
pp	2	0	$\Sigma^-\Sigma^0$	-1	-2	$\Xi^-\Sigma^0$	-1	-3
$n\Sigma^-$	-1	-1	$n\Xi^-$			$\Xi^-\Lambda$		
$n\Lambda$			$\Sigma^+\Sigma^-$			$\Xi^-\Sigma^+$		
$n\Sigma^0$	0	-1	$\Sigma^0\Sigma^0$			$\Xi^0\Lambda$	0	-3
$p\Sigma^-$			$\Lambda\Sigma^0$			$\Xi^0\Sigma^0$		
$p\Lambda$			$\Lambda\Lambda$	0	-2	$\Xi^0\Sigma^+$	1	-3
$p\Sigma^0$	1	-1	$n\Xi^0$			$\Xi^-\Xi^-$	-2	-4
$n\Sigma^+$			$p\Xi^-$			$\Xi^-\Xi^0$	-1	-4
$p\Sigma^+$	2	-1	$\Sigma^+\Lambda$			$\Xi^0\Xi^0$	0	-4
			$\Sigma^+\Sigma^0$	1	-2			
			$p\Xi^0$					
			$\Sigma^+\Sigma^+$	2	-2			

TABLE I. The charge and strangeness of baryon pairs. Strangeness decreases and charge increases from top to bottom.

Baryon pairs	symmetric flavor irrep	anti-symmetric flavor irrep
$np, \Sigma^-\Xi^-, \Sigma^+\Xi^0$	27	$\overline{\mathbf{10}}$
$n\Sigma^-, p\Sigma^+, \Xi^-\Xi^0$	27	10

TABLE II. The baryon pairs in one-dimensional subspaces of S and Q values, and the flavor irreps they sit in.

irreps, as shown in Table II. The S -matrix is the same as in Eq. (33) with $\delta_0 = \delta_{\mathbf{27}}$ and $\delta_1 = \delta_{\mathbf{10}}$ for the pairs $\{np, \Sigma^-\Xi^-, \Sigma^+\Xi^0\}$, while $\delta_1 = \delta_{\overline{\mathbf{10}}}$ for $\{n\Sigma^-, p\Sigma^+, \Xi^-\Xi^0\}$.

For three-dimensional subspaces, the irreps involved are **27**, $\mathbf{8_S}$, $\mathbf{8_A}$, **10** and $\overline{\mathbf{10}}$. (We list all the flavor eigenstates, i.e., states with definite Q and S , within each irrep in Appendix B.) The S -matrix can be written in the form,

$$S = \frac{1 - \boldsymbol{\sigma} \cdot \boldsymbol{\sigma}}{4} \otimes (\mathbf{P}_{\mathbf{27}} e^{2i\delta_{\mathbf{27}}} + \mathbf{P}_{\mathbf{8_S}} e^{2i\delta_{\mathbf{8_S}}}) + \frac{3 + \boldsymbol{\sigma} \cdot \boldsymbol{\sigma}}{4} \otimes (\mathbf{P}_{\mathbf{10}} e^{2i\delta_{\mathbf{10}}} + \mathbf{P}_{\overline{\mathbf{10}}} e^{2i\delta_{\overline{\mathbf{10}}}} + \mathbf{P}_{\mathbf{8_A}} e^{2i\delta_{\mathbf{8_A}}}), \quad (37)$$

where $\mathbf{P}_{\mathbf{27}}$ is a projection operator onto the **27** irrep in the flavor space, etc. Again only flavor-symmetric irreps appear in the 1S_0 channel; the flavor-antisymmetric irreps reside in the 3S_1 channel.

The projection operators can be worked out as follows, using the $(Q, S) = (0, -1)$ sector spanned by $\{\Sigma^0 n, \Sigma^- p, \Lambda n\}$ as an illustration. From Appendix B, we see baryon pairs in

this sector have components in several irreps:

$$|\mathbf{27}\rangle = \sqrt{\frac{2}{3}} |\Sigma^0 n\rangle_S + \sqrt{\frac{1}{3}} |\Sigma^- p\rangle_S , \quad (38)$$

$$|\mathbf{27}'\rangle = -\sqrt{\frac{1}{30}} |\Sigma^0 n\rangle_S + \sqrt{\frac{1}{15}} |\Sigma^- p\rangle_S + \sqrt{\frac{9}{10}} |\Lambda n\rangle_S , \quad (39)$$

$$|\mathbf{8_S}\rangle = \sqrt{\frac{3}{10}} |\Sigma^0 n\rangle_S - \sqrt{\frac{3}{5}} |\Sigma^- p\rangle_S + \sqrt{\frac{1}{10}} |\Lambda n\rangle_S , \quad (40)$$

$$|\mathbf{10}\rangle = \sqrt{\frac{2}{3}} |\Sigma^0 n\rangle_A + \sqrt{\frac{1}{3}} |\Sigma^- p\rangle_A , \quad (41)$$

$$|\overline{\mathbf{10}}\rangle = -\sqrt{\frac{1}{6}} |\Sigma^0 n\rangle_A + \sqrt{\frac{1}{3}} |\Sigma^- p\rangle_A + \sqrt{\frac{1}{2}} |\Lambda n\rangle_A , \quad (42)$$

$$|\mathbf{8_A}\rangle = -\sqrt{\frac{1}{6}} |\Sigma^0 n\rangle_A + \sqrt{\frac{1}{3}} |\Sigma^- p\rangle_A - \sqrt{\frac{1}{2}} |\Lambda n\rangle_A , \quad (43)$$

where the S and A subscripts denote symmetrized and anti-symmetrized flavor quantum numbers states, respectively,

$$|F_1 F_2\rangle_{S/A} \equiv \frac{1}{\sqrt{2}} (|F_1\rangle \otimes |F_2\rangle \pm |F_2\rangle \otimes |F_1\rangle) . \quad (44)$$

Equations (38) - (43) define an $SU(3)$ -flavor basis, in which the flavor part of the S -matrix in the R -irrep must be proportional to $e^{2i\delta_R} \mathbf{1}$.⁸ In this basis the projectors in the S -matrix are all diagonal, similar to the np scattering in the isospin basis in Eq. (34),

$$P_{\mathbf{27}} = \text{Diag} (1, 0, 0, 0, 0, 0) , \quad (45)$$

$$P'_{\mathbf{27}} = \text{Diag} (0, 1, 0, 0, 0, 0) , \quad (46)$$

$$P_{\mathbf{8_S}} = \text{Diag} (0, 0, 1, 0, 0, 0) , \quad (47)$$

$$P_{\mathbf{10}} = \text{Diag} (0, 0, 0, 1, 0, 0) , \quad (48)$$

$$P_{\overline{\mathbf{10}}} = \text{Diag} (0, 0, 0, 0, 1, 0) , \quad (49)$$

$$P_{\mathbf{8_A}} = \text{Diag} (0, 0, 0, 0, 0, 1) . \quad (50)$$

These projection operators satisfy the relations: $\sum_R P_R = 1$ and $P_R P_{R'} = \delta_{RR'} P_R$.

A physical scattering process takes as an initial state one of the states from the flavor eigenbasis consisting of $\{|\Sigma^0 n\rangle, |\Sigma^- p\rangle, |\Lambda n\rangle, |n\Sigma^0\rangle, |p\Sigma^-\rangle, |n\Lambda\rangle\}$. In this physical basis the

⁸ Recall that the S -matrix must be invariant under $SU(3)$ rotations in the respective irrep.

projection operator P_R becomes

$$P_R \rightarrow O^\dagger P_R O, \quad O = \left(\begin{array}{c|c} \frac{1}{\sqrt{2}}P_S & \frac{1}{\sqrt{2}}P_S \\ \hline \frac{1}{\sqrt{2}}P_A & -\frac{1}{\sqrt{2}}P_A \end{array} \right), \quad (51)$$

where O is the generalization of Eq. (36) with

$$P_S = \begin{pmatrix} \sqrt{2/3} & \sqrt{1/3} & 0 \\ -\sqrt{1/30} & \sqrt{1/15} & \sqrt{9/10} \\ \sqrt{3/10} & -\sqrt{3/5} & \sqrt{1/10} \end{pmatrix}, \quad P_A = \begin{pmatrix} \sqrt{2/3} & \sqrt{1/3} & 0 \\ -\sqrt{1/6} & \sqrt{1/3} & \sqrt{1/2} \\ -\sqrt{1/6} & \sqrt{1/3} & -\sqrt{1/2} \end{pmatrix}. \quad (52)$$

For the 6-dim sector listed in Table I, the construction of the S -matrix proceeds similarly. In Appendix B we provide the $SU(3)$ basis in all flavor sectors. The basis transformation matrices P_S and P_A in each sector can be read off from the tables in Appendix B.

C. Minimally entangling S -matrix

To study the entanglement property of the S -matrix, it will be illuminating to again first consider the nucleon-nucleon channel. In this regard we will rewrite Eq. (31) in terms of the Identity and SWAP operator defined in Eq. (9),

$$S = \frac{1 - \text{SWAP}}{2} \otimes \frac{1 + \overline{\text{SWAP}}}{2} e^{2i\delta_0} + \frac{1 + \text{SWAP}}{2} \otimes \frac{1 - \overline{\text{SWAP}}}{2} e^{2i\delta_1}, \quad (53)$$

where $\overline{\text{SWAP}} \equiv (1 + \boldsymbol{\tau} \cdot \boldsymbol{\tau})/2$ is the SWAP operator acting in the flavor space. Now if we set $\delta_0 = \delta_1 = \delta$,

$$S = \frac{e^{2i\delta}}{2} (1 \otimes 1 - \text{SWAP} \otimes \overline{\text{SWAP}}) = e^{2i\delta} 1 \otimes 1, \quad (54)$$

where we have used the fact that $\text{SWAP} \otimes \overline{\text{SWAP}} = -1 \otimes 1$ due to Fermi-Dirac statistics,

$$\text{SWAP} \otimes \overline{\text{SWAP}} |N_1, s_1; N_2, s_2\rangle = |N_2, s_2; N_1, s_1\rangle = -|N_1, s_1; N_2, s_2\rangle. \quad (55)$$

So the S -matrix is an Identity gate in both the spin and the flavor space! Moreover, the emergent $SU(4)_{sm}$ spin-flavor symmetry is evident since S -matrix is proportional to the

Identity. Similarly, if $\delta_1 = \delta_0 \pm \pi/2 = \delta$,

$$S = \frac{e^{2i\delta}}{2} (\text{SWAP} \otimes 1 - 1 \otimes \overline{\text{SWAP}}) = e^{2i\delta} \text{SWAP} \otimes 1 , \quad (56)$$

where the Fermi-Dirac Statistics again implies

$$1 \otimes \overline{\text{SWAP}} |N_1, s_1; N_2, s_2\rangle = -\text{SWAP} \otimes 1 |N_1, s_1; N_2, s_2\rangle . \quad (57)$$

In this case, the S -matrix is a SWAP gate in the spin space and an Identity in the flavor space or, equivalently, an Identity in the spin and a SWAP in the flavor.

The discussion above highlights the interplay of entanglement in the spin subspace and in the flavor subspace, in the presence of Fermi-Dirac statistics: the ability of the S -matrix to generate entanglement in the spin space is equivalent to the ability to entangle in the flavor space. This is most clear when considering the operator $1 \otimes (1 + \overline{\text{SWAP}})$, which entangles flavor but not spin. However, using Eq. (57) we see

$$1 \otimes (1 + \overline{\text{SWAP}}) = (1 - \text{SWAP}) \otimes 1 , \quad (58)$$

which now entangles the spin but not flavor.

More generally, the S -matrix in baryon-baryon scattering can be written as

$$S = \frac{1}{2} \sum_{\substack{R \in \{\mathbf{27}, \mathbf{8}_S, \mathbf{1}\} \\ R' \in \{\mathbf{10}, \mathbf{10}, \mathbf{8}_A\}}} \left[1 \otimes (P_R e^{2i\delta_R} + P_{R'} e^{2i\delta_{R'}}) - \text{SWAP} \otimes (P_R e^{2i\delta_R} - P_{R'} e^{2i\delta_{R'}}) \right] . \quad (59)$$

where some irreps are absent in 3-dim and 1-dim sectors. Comparison with Eqs. (54) and (56) suggests that the S -matrix in the above equation is minimally entangling if one of the two following conditions are satisfied,

$$S \propto \frac{1}{2} (1 \otimes 1 - \text{SWAP} \otimes \overline{\text{SWAP}}) = 1 \otimes 1 , \quad (60)$$

$$S \propto \frac{1}{2} (\text{SWAP} \otimes 1 - 1 \otimes \overline{\text{SWAP}}) = \text{SWAP} \otimes 1 . \quad (61)$$

Let's consider the two possibilities in turn.

The first possibility is achieved when

$$\sum_R P_R e^{2i\delta_R} + \sum_{R'} P_{R'} e^{2i\delta_{R'}} = e^{2i\delta_I} \mathbf{1} , \quad (62)$$

$$\sum_R P_R e^{2i\delta_R} - \sum_{R'} P_{R'} e^{2i\delta_{R'}} = e^{2i\delta_I} \overline{\text{SWAP}} , \quad (63)$$

where δ_I is an arbitrary phase shift. To solve for these two relations it is more convenient to choose the $SU(3)$ -symmetric basis for the flavor subspace, for examples Eqs. (38) - (43), in which the projection operator takes particularly simple forms, as shown in Eqs. (45) - (50). In this basis the $\overline{\text{SWAP}}$ is also simple because the $SU(3)$ -symmetric states are eigenstates of $\overline{\text{SWAP}}$:

$$\overline{\text{SWAP}} |R\rangle = |R\rangle \quad \text{for} \quad R \in \{\mathbf{27}, \mathbf{8}_S, \mathbf{1}\} , \quad (64)$$

$$\overline{\text{SWAP}} |R'\rangle = -|R'\rangle \quad \text{for} \quad R' \in \{\mathbf{10}, \overline{\mathbf{10}}, \mathbf{8}_A\} , \quad (65)$$

where the eigenvalues are +1 for the flavor symmetric irreps and -1 for the flavor antisymmetric irreps. More explicitly, in the basis of Eqs. (38) - (43), the relations in Eqs. (62) and (63) become

$$\sum_R P_R e^{2i\delta_R} + \sum_{R'} P_{R'} e^{2i\delta_{R'}} = e^{2i\delta_I} \left(\begin{array}{c|c} \mathbf{1}_3 & \\ \hline & \mathbf{1}_3 \end{array} \right) , \quad (66)$$

$$\sum_R P_R e^{2i\delta_R} - \sum_{R'} P_{R'} e^{2i\delta_{R'}} = e^{2i\delta_I} \left(\begin{array}{c|c} \mathbf{1}_3 & \\ \hline & -\mathbf{1}_3 \end{array} \right) , \quad (67)$$

where $\mathbf{1}_3$ is a 3×3 Identity matrix. From the matrix representations of $P_{R/R'}$ in Eqs. (45) - (50), it is easy to see the solution for the above equation is when all the scattering phases are equal:

$$\delta_R = \delta_{R'} \equiv \delta_I \quad \Rightarrow \quad S = e^{2i\delta_I} \mathbf{1} \otimes \mathbf{1} . \quad (68)$$

So the solution for an Identity gate in the np scattering generalizes to the baryon scattering.

Next we consider the second possibility, which is reached through the relations

$$\sum_R P_R e^{2i\delta_R} + \sum_{R'} P_{R'} e^{2i\delta_{R'}} = e^{2i\delta_S} \overline{\text{SWAP}} , \quad (69)$$

(Q, S) sectors	Minimal entanglement conditions
np $\Sigma^-\Xi^-$ $\Sigma^+\Xi^0$	$\delta_{27} = \delta_{\overline{10}}$ or $\delta_{27} = \delta_{\overline{10}} \pm \frac{\pi}{2}$
$n\Sigma^-$ $p\Sigma^+$ $\Xi^-\Xi^0$	$\delta_{27} = \delta_{10}$ or $\delta_{27} = \delta_{10} \pm \frac{\pi}{2}$
$(p\Lambda, p\Sigma^0, n\Sigma^+)$ $(n\Lambda, n\Sigma^0, p\Sigma^-)$ $(\Sigma^-\Lambda, \Sigma^-\Sigma^0, n\Xi^-)$ $(\Sigma^+\Lambda, \Sigma^+\Sigma^0, p\Xi^0)$ $(\Sigma^-\Xi^0, \Xi^-\Sigma^0, \Xi^-\Sigma^0)$ $(\Xi^-\Sigma^+, \Xi^0\Lambda, \Xi^0\Sigma^0)$	$\delta_{27} = \delta_{8_S} = \delta_{10} = \delta_{\overline{10}} = \delta_{8_A}$ or $\delta_{27} = \delta_{8_S} = \delta_{10} \pm \frac{\pi}{2} = \delta_{\overline{10}} \pm \frac{\pi}{2} = \delta_{8_A} \pm \frac{\pi}{2}$
$(\Sigma^+\Sigma^-, \Sigma^0\Sigma^0, \Lambda\Sigma^0, \Xi^-p, \Xi^0n, \Lambda\Lambda)$	$\delta_{27} = \delta_{8_S} = \delta_1 = \delta_{10} = \delta_{\overline{10}} = \delta_{8_A}$ or $\delta_{27} = \delta_{8_S} = \delta_1 = \delta_{10} \pm \frac{\pi}{2} = \delta_{\overline{10}} \pm \frac{\pi}{2} = \delta_{8_A} \pm \frac{\pi}{2}$

TABLE III. Conditions in each flavor sector for the S -matrix to be minimally entangling. An Identity gate is achieved when all the phases are equal, while a SWAP gate is when the phases differ by $\pi/2$.

$$\sum_R P_R e^{2i\delta_R} - \sum_{R'} P_{R'} e^{2i\delta_{R'}} = e^{2i\delta_S} 1 . \quad (70)$$

Again in the $SU(3)$ -symmetric basis the solution is when

$$\delta_R \equiv \delta_S = \delta_{R'} \pm \frac{\pi}{2} \quad \Rightarrow \quad S = e^{2i\delta_S} \text{SWAP} \otimes 1 . \quad (71)$$

Again this is a generalization of the solution leading to the SWAP gate in np scattering.

In Table. III we list the explicit solutions for the S -matrix to be minimally entangling for each (Q, S) sector.

VI. ENTANGLEMENT MINIMUM AND SYMMETRY

In this Section we investigate the possible emergent symmetries in the EFT when the S -matrix is minimally entangling. The Lagrangian for the EFT is given in Eq. (23). It will be convenient to project the contact operators into irreps of $SU(3)$ flavor symmetry and the corresponding $SU(3)$ -symmetric Wilson coefficients are [6]:

$$C_{27} = c_1 - c_2 + c_5 - c_6 , \quad (72)$$

$$C_{\mathbf{8}_S} = -\frac{2}{3}c_1 + \frac{2}{3}c_2 - \frac{5}{6}c_3 + \frac{5}{6}c_4 + c_5 - c_6 , \quad (73)$$

$$C_{\mathbf{1}} = -\frac{1}{3}c_1 + \frac{1}{3}c_2 - \frac{8}{3}c_3 + \frac{8}{3}c_4 + c_5 - c_6 , \quad (74)$$

$$C_{\overline{\mathbf{10}}} = c_1 + c_2 + c_5 + c_6 , \quad (75)$$

$$C_{\mathbf{10}} = -c_1 - c_2 + c_5 + c_6 , \quad (76)$$

$$C_{\mathbf{8}_A} = \frac{3}{2}c_3 + \frac{3}{2}c_4 + c_5 + c_6 . \quad (77)$$

At the leading order in EFT, the relation between the Wilson coefficient C_i and the scattering phase δ_i is simple and given by Eqs. (13) and (19),

$$p \cot \delta_i = - \left(\mu + \frac{4\pi}{MC_i} \right) , \quad (78)$$

where the natural scattering length is recovered by setting $\mu = 0$. The conditions for a minimally entangling S -matrix in Eqs. (68) and (71) translate directly into constraints on the Wilson coefficients,

$$\delta_R = \delta_{R'} \quad \Longrightarrow \quad C_R = C_{R'} \quad (\text{natural and unnatural}) , \quad (79)$$

$$\delta_R = \delta_{R'} \pm \frac{\pi}{2} \quad \Longrightarrow \quad \begin{cases} C_R = -\frac{4\pi}{M\mu} , C_{R'} = 0 \\ C_R = 0 , C_{R'} = -\frac{4\pi}{M\mu} \end{cases} \quad (\text{unnatural}) . \quad (80)$$

There are no values of C_i that allow the $\pi/2$ phase difference in the natural scattering length case. Moreover, the values of $C_{R,R'}$ in the unnatural $\pi/2$ phase difference case set $\delta_R = 0, \delta_{R'} = \pi/2$ or vice versa. When the scattering phase $\delta = \pi/2$, the scattering length becomes infinite and the channel exhibits the Schrödinger symmetry. In this case the channel reaches the unitarity limit. When the phase $\delta = 0$, the S -matrix corresponds to a free theory and is also invariant under the Schrödinger group. In Table IV we list the corresponding constraints on the Wilson coefficients for each (Q, S) sector, as deduced from Table III.

The previous discussion concerns minimal entanglement in a particular (Q, S) sector and the constraints in Eqs. (79) and (80) apply to only a subset of irreps of $\mathbf{8} \otimes \mathbf{8}$ that are involved, except for the 6-dim $(Q, S) = (0, -2)$ sector, where all six irreps enter. In this case, minimal entanglement in the 6-dim sector forces minimal entanglement in all other (Q, S) sectors for scattering of non-identical baryons. This is the the global entanglement

Flavor subspaces	Minimal entanglement conditions
np $\Sigma^-\Xi^-$ $\Sigma^+\Xi^0$	$c_2 = -c_6$ or $c_1 + c_5 = -\frac{2\pi}{M\mu}, c_2 + c_6 = \pm\frac{2\pi}{M\mu}$
$n\Sigma^-$ $p\Sigma^+$ $\Xi^-\Xi^0$	$c_1 = c_6$ or $-c_2 + c_5 = -\frac{2\pi}{M\mu}, c_1 - c_6 = \pm\frac{2\pi}{M\mu}$
$(p\Lambda, p\Sigma^0, n\Sigma^+)$ $(n\Lambda, n\Sigma^0, p\Sigma^-)$ $(\Sigma^-\Lambda, \Sigma^-\Sigma^0, n\Xi^-)$ $(\Sigma^+\Lambda, \Sigma^+\Sigma^0, p\Xi^0)$ $(\Sigma^-\Xi^0, \Xi^-\Sigma^0, \Xi^-\Sigma^0)$ $(\Xi^-\Sigma^+, \Xi^0\Lambda, \Xi^0\Sigma^0)$	$c_1 = -c_2 = -\frac{1}{2}c_3 = \frac{1}{2}c_4 = c_6$ or $c_1 = -c_2 = -\frac{1}{2}c_3 = \frac{1}{2}c_4 = -c_5 - \frac{2\pi}{M\mu} = c_6 \pm \frac{2\pi}{M\mu}$
$(\Sigma^+\Sigma^-, \Sigma^0\Sigma^0, \Lambda\Sigma^0, \Xi^-p, \Xi^0n, \Lambda\Lambda)$	$c_1 = c_2 = c_3 = c_4 = c_6 = 0$ or $c_1 = c_2 = c_3 = c_4 = 0, c_5 = -\frac{2\pi}{M\mu}, c_6 = \pm\frac{2\pi}{M\mu}$

TABLE IV. Minimal entanglement conditions on Wilson coefficients in each flavor subspace.

minimum and the constraints are

$$\delta_R = \delta_{R'}, \quad \forall R, R' \implies c_1 = c_2 = c_3 = c_4 = c_6 = 0, \quad c_5 \text{ unconstrained}, \quad (81)$$

$$\delta_R = \delta_{R'} \pm \frac{\pi}{2}, \quad \forall R, R' \implies c_1 = c_2 = c_3 = c_4 = 0, \quad c_5 = -\frac{2\pi}{M\mu}, \quad c_6 = \pm\frac{2\pi}{M\mu}, \quad (82)$$

where the first line applies to both natural and unnatural cases, and the second line only applies to the unnatural case. The first condition was first reported in Ref. [1] and leads to the emergent $SU(16)_{sm}$ spin-flavor symmetry. The second condition results in the S -matrix being a SWAP operator in either the spin or the flavor space and we expect Schrödinger symmetry to emerge, similarly to the case of np scattering that was first reported in Ref. [23].

Next we will use the EFT Lagrangian to investigate the emergent symmetries associated with the conditions listed in Table IV, starting from the 1-dim sectors and then moving toward the global minimum at the 6-dim sector.

A. Minimal entanglement in 1-dim sectors – $SU(6)$

As shown in Table. II, there are two different classes of 1-dim sectors: $\{n\Sigma^-, p\Sigma^+, \Xi^-\Xi^0\}$ involves $\mathbf{10}$ and $\{np, \Sigma^-\Xi^-, \Sigma^+\Xi^0\}$ contains $\overline{\mathbf{10}}$. Recall that $\mathbf{10}$ and $\overline{\mathbf{10}}$ are irreps of $SU(3)$

related by complex conjugation, under which $(Q, S + 1) \rightarrow (-Q, -(S + 1))$. This can also be seen from the “eight-fold way” in Fig. 2, where the action of complex conjugate gives $n \leftrightarrow \Xi^0$, $p \leftrightarrow \Xi^-$ and $\Sigma^+ \leftrightarrow \Sigma^-$.

Let us consider $\{n\Sigma^-, p\Sigma^+, \Xi^-\Xi^0\}$ first. Minimizing the entanglement in this class requires $C_{27} = C_{\overline{10}}$. This turns out to be a prediction of the $SU(6)$ spin-flavor symmetry which combines the two spin states with the three quark flavors (u, d, s) into a fundamental representation $(\mathbf{6})$ of $SU(6)$, whose corresponding Lagrangian in Eq. (25) contains only two parameters a and b . Re-expressing the $SU(3)$ -symmetric Wilson coefficients using Eqs. (26) - (28), we find

$$C_{27} = a - \frac{1}{27}b, \quad C_{\mathbf{8}_S} = a + \frac{1}{3}b, \quad C_{\mathbf{1}} = a - \frac{1}{3}b, \quad (83)$$

$$C_{\mathbf{10}} = a + \frac{7}{27}b, \quad C_{\overline{\mathbf{10}}} = a - \frac{1}{27}b, \quad C_{\mathbf{8}_A} = a + \frac{1}{27}b. \quad (84)$$

Thus $SU(6)$ symmetry predicts

$$C_{27} = C_{\overline{10}} \quad \Rightarrow \quad \delta_{27} = \delta_{\overline{10}}, \quad (85)$$

leading to minimal entanglement in all three channels in $\{n\Sigma^-, p\Sigma^+, \Xi^-\Xi^0\}$. In principle there are three other linear relations among the $SU(3)$ -symmetric Wilson coefficients following from the $SU(6)$ spin-flavor symmetry, although they do not seem to lead to entanglement suppression in other channels.

On the other hand, requiring minimal entanglement in $\{np, \Sigma^-\Xi^-, \Sigma^+\Xi^0\}$ gives $C_{27} = C_{\mathbf{10}}$, which is not a prediction of $SU(6)$. However, since $\{np, \Sigma^-\Xi^-, \Sigma^+\Xi^0\}$ channels are the complex conjugate of $\{\Xi^-\Xi^0, p\Sigma^+, n\Sigma^-\}$, one can see that $C_{27} = C_{\mathbf{10}}$ is a prediction of $\overline{SU(6)}$, where the two spin states together with (u, d, s) quarks now transform as the anti-fundamental representation $(\overline{\mathbf{6}})$ of $SU(6)$.

B. Minimal entanglement in 3-dim sectors – $SO(8)$

As seen from Table IV, in 3-dim flavor sectors the Identity gate is achieved when $c_1 = -c_2 = -\frac{1}{2}c_3 = \frac{1}{2}c_4 = c_6$. Quite unexpectedly, the Lagrangian in Eq. (23) simplifies upon

the use of the Cayley-Hamilton theorem in Eq. (24):

$$\mathcal{L} = -(c_1 + c_5) \langle B_i^\dagger B_i \rangle \langle B_j^\dagger B_j \rangle + c_1 \langle B_i^\dagger B_j^\dagger \rangle \langle B_i B_j \rangle . \quad (86)$$

The above Lagrangian has an emergent $SO(8)$ symmetry. This is the easiest to see by projecting the baryon matrix B in Eq. (22) into $SU(3)$ generators T^a which satisfy $[T^a, T^b] = if^{abc}T^c$ and $\text{Tr}(T^a T^b) = \frac{1}{2}\delta^{ab}$,

$$B^a \equiv \text{Tr}(BT^a) , \quad a = 1, \dots, 8 , \quad (87)$$

$$\begin{aligned} \vec{B} &= (B^1, \dots, B^8) \\ &= \frac{1}{2} \left(\Sigma^+ + \Sigma^-, i\Sigma^+ - i\Sigma^-, p + \Xi^-, ip - i\Xi^-, n + \Xi^0, in - i\Xi^0, \sqrt{2}\Sigma^0, \sqrt{2}\Lambda \right) , \end{aligned} \quad (88)$$

where we have chosen $T^a = \lambda^a/2$, where $\lambda^a, a = 1, \dots, 8$ are the famed Gell-Mann matrices for the $SU(3)$ eight-fold way [24]. Then the Lagrangian becomes

$$\mathcal{L} = -2(c_1 + c_5) \left(\vec{B}_i^\dagger \cdot \vec{B}_i \right) \left(\vec{B}_j^\dagger \cdot \vec{B}_j \right) + 2c_1 \left(\vec{B}_i^\dagger \cdot \vec{B}_j^\dagger \right) \left(\vec{B}_i \cdot \vec{B}_j \right) , \quad (89)$$

where we recall the i, j indices represents the two spin states of the baryon. In this notation the first operator in Eq. (89) preserves an $SU(8)$ flavor symmetry,

$$\vec{B} \rightarrow \mathcal{U}\vec{B} , \quad \mathcal{U}^\dagger \mathcal{U} = 1 . \quad (90)$$

However, the second operator is invariant only under an $SO(8)$ subgroup of $SU(8)$:⁹

$$\vec{B} \rightarrow \mathcal{O}\vec{B} , \quad \mathcal{O}^T \mathcal{O} = 1 , \quad \text{where } \mathcal{O} \in SO(8) . \quad (91)$$

Thus the Lagrangian in Eq. (89) is invariant under an emergent $SO(8)$ symmetry.

⁹ Group generators of $SU(N)$ are $N \times N$ traceless Hermitian matrices, among which the purely imaginary ones are antisymmetric and hence generators of the $SO(N)$ subgroup.

Flavor subspace	Symmetry of Lagrangian
np $\Sigma^-\Xi^-$ $\Sigma^+\Xi^0$	$SU(6)$ spin-flavor symmetry or Schrödinger symmetry in 27 and $\overline{\mathbf{10}}$ irrep channels
$n\Sigma^-$ $p\Sigma^+$ $\Xi^-\Xi^0$	conjugate of $SU(6)$ spin-flavor symmetry or Schrödinger symmetry in 27 and 10 irrep channels
$(p\Lambda, p\Sigma^0, n\Sigma^+)$ $(n\Lambda, n\Sigma^0, p\Sigma^-)$ $(\Sigma^-\Lambda, \Sigma^-\Sigma^0, n\Xi^-)$ $(\Sigma^+\Lambda, \Sigma^+\Sigma^0, p\Xi^0)$ $(\Sigma^-\Xi^0, \Xi^-\Sigma^0, \Xi^-\Sigma^0)$ $(\Xi^-\Sigma^+, \Xi^0\Lambda, \Xi^0\Sigma^0)$	$SO(8)$ flavor symmetry or Schrödinger symmetry in 27 , 8_S , 8_A , 10 and $\overline{\mathbf{10}}$ irrep channels
$(\Sigma^+\Sigma^-, \Sigma^0\Sigma^0, \Lambda\Sigma^0, \Xi^-p, \Xi^0n, \Lambda\Lambda)$	$SU(16)$ symmetry or $SU(8)$ and Schrödinger symmetry

TABLE V. Symmetries predicted by entanglement minimization in each flavor sector.

C. Minimal entanglement in 6-dim sector – $SU(8)$ and $SU(16)$

When the global entanglement is minimized, c_1 – c_4 operators all vanish, and only c_5 and c_6 operators are present, depending on whether the scattering is natural or unnatural. In the case of a natural scattering length, only c_5 is non-zero and the Lagrangian is

$$\mathcal{L} = -c_5 \langle B_i^\dagger B_i \rangle \langle B_j^\dagger B_j \rangle . \quad (92)$$

As reported in Ref. [1] this Lagrangian has an $SU(16)$ global symmetry:

$$\mathcal{B} = (n_\uparrow, n_\downarrow, p_\uparrow, p_\downarrow, \dots) , \quad \mathcal{L} = -c_5 (\mathcal{B}^\dagger \mathcal{B})^2 . \quad (93)$$

When both c_5 and c_6 are non-zero, as in the case of an unnatural scattering length,

$$\begin{aligned} \mathcal{L} &= -c_5 \langle B_i^\dagger B_i \rangle \langle B_j^\dagger B_j \rangle - c_6 \langle B_i^\dagger B_j \rangle \langle B_i^\dagger B_j \rangle \\ &= -2c_5 \left(\vec{B}_i^\dagger \cdot \vec{B}_i \right) \left(\vec{B}_j^\dagger \cdot \vec{B}_j \right) - 2c_6 \left(\vec{B}_i^\dagger \cdot \vec{B}_j \right) \left(\vec{B}_i^\dagger \cdot \vec{B}_j \right) . \end{aligned} \quad (94)$$

From the reasoning in Section VI B, one sees that the $SU(8)$ symmetry exhibited in Eq. (90) leaves the above Lagrangian invariant. The $SU(8)$ flavor symmetry is in addition to the non-relativistic conformal invariance that is present when c_5 and c_6 flows to the UV fixed

	$C_{\mathbf{27}}$	$C_{\mathbf{10}}$	$C_{\overline{\mathbf{10}}}$	$C_{\mathbf{8_A}}$
natural [6]	-16.7(2.8)	-50(50)	-11.1(2.5)	-7.7(1.8)
unnatural [6]	1.89(4)	1.75(6)	2.00(8)	2.17(9)
natural [25]	-28_{-5}^{+3}	-	-29_{-4}^{+3}	-19_{-1}^{+1}
unnatural [25]	$10.0_{-0.5}^{+0.5}$	-	$11.3_{-0.5}^{+0.5}$	$12.8_{-0.5}^{+0.5}$

TABLE VI. Wilson coefficients of each irrep, in lattice units, from data in Refs. [6, 25], where $\mu = m_\pi = 806$ MeV and 450 MeV, respectively, in the simulations. For $C_{\mathbf{27}}$ there are several values obtained from different channels and methods listed in Ref. [25]. We picked one with the smallest error bar as a representative.

point. The full symmetry predictions following from entanglement minimization are listed in Table. V.

VII. RESULTS FROM LATTICE QCD

In QCD baryon-baryon interactions were simulated numerically by the NPLQCD Collaboration and four out of the six scattering lengths in $SU(3)$ -symmetric channels were evaluated in Ref. [6] for both natural scattering length ($\mu = 0$) and unnatural scattering length ($\mu = m_\pi$), where $m_\pi = 806$ MeV is the mass of the pion in the simulation. More recently new simulations with a more realistic pion mass, $m_\pi = 450$ MeV, have appeared in Ref. [25] for three out of the six channels.

We list the values of C_R from Refs. [6, 25] in Table. VI. Focusing on simulations with $m_\pi = 806$ MeV in Ref. [6] for now, we see that, in the case of unnatural scattering length, $C_{\mathbf{27}} \approx C_{\mathbf{10}} \approx C_{\overline{\mathbf{10}}} \approx C_{\mathbf{8_A}}$. These results imply the presence of $SU(6)$ spin-flavor symmetry, which can then be used to deduce the other two Wilson coefficients $C_{\mathbf{8_S}}$ and $C_{\mathbf{1}}$ using Eqs. (26) - (28). In the end the Wilson coefficients in all $SU(3)$ -symmetric channels are all approximately in the same numerical range, a strong indicator of $SU(16)$ spin-flavor symmetry. On the other hand, in simulations using more realistic $m_\pi = 450$ MeV in Ref. [25], only three channels are provided, among which the $SU(6)$ predictions seem to continue to hold up well. In the case of natural scattering length, $SU(6)$ spin-flavor symmetry requires $C_{\mathbf{27}} \approx C_{\overline{\mathbf{10}}}$ or $C_{\mathbf{27}} \approx C_{\mathbf{10}}$, without which the other two Wilson coefficients cannot be deduced. As can be seen from Table VI, $C_{\mathbf{27}} \approx C_{\overline{\mathbf{10}}}$ seems to work in Ref. [25], where a lower m_π is employed.

At this point it is clear that no firm conclusion can be drawn from the lattice data. It

would be desirable to improve on the precision of lattice simulation, as well as computing the Wilson coefficients in more $SU(3)$ -symmetric channels, in order to gain further insights on the possible emergent symmetries in low-energy QCD.

VIII. CONCLUSION

In this paper, building upon the work of Refs. [1, 2], we showed that successive entanglement minimization in $SU(3)$ -symmetric channels lead to increasingly large emergent symmetries in low-energy interactions of spin-1/2 baryons, as demonstrated in Table V. Our findings strongly hint at a new paradigm where symmetry can be considered as the outgrowth of entanglement minimization. With the benefit of hindsight, it may not seem surprising that there is a correlation between entanglement and symmetry since, from the thermodynamic point of view, both are related to the presence of “order” (or the lack thereof) in the physical system.¹⁰ This paper represents a first step in establishing a quantitative relation between entanglement and symmetry.

There are many other questions to be answered before we can fully grasp the implications of results in this work. We have considered emergent global symmetries in low-energy QCD. It would be natural to explore similar connections in other physical systems, for example few-body systems in atomic, molecular, and optical (AMO) physics, as well as other types of symmetries such as the gauge symmetry.¹¹ In addition, global symmetries considered in this work are realized in the Wigner-Weyl mode, where the spectrum of the dynamical system furnishes linear representations of the symmetry group. It would be interesting to understand the Nambu-Goldstone mode, commonly referred to as spontaneous symmetry breaking, from the perspective of quantum information science.¹²

Entanglement may also provide a new context to understand another long-standing puzzle in fundamental physics: whether nature is fine tuned. The large scattering length in np scattering in the 3S_1 channel gives rise to a near-threshold bound state – the deuteron – whose existence is often attributed to fine tuning: the binding energy of deuteron is only 2.2 MeV, smaller than the typical nuclear binding of $\mathcal{O}(10)$ MeV. On the other hand, we now

¹⁰ Recall that the von Neumann entropy in Eq. (1) is an entanglement measure.

¹¹ For an exploratory study in this direction, see Ref. [26].

¹² See Ref. [11] for an initial study.

know that the large scattering length is associated with the S -matrix realizing the SWAP gate. It remains to be seen whether other fine-tuned systems can be understood in a similar fashion.

Last but not least, insights into the precise relation between entanglement and symmetry may in the long run help us devise efficient quantum algorithms to simulate physical systems with a certain type of symmetry. Given the ubiquitous presence of symmetries in nature, this may have broad applications.

ACKNOWLEDGMENTS

I.L. is supported by the U.S. Department of Energy, Office of Science, Office of Nuclear Physics under Grant No. DE-SC0023522. Q.L. is supported by a University Fellowship from The Graduate School at Northwestern University. T.M. is supported by the U.S. Department of Energy, Office of Science, Office of Nuclear Physics under grant Contract No. DE-FG02-05ER41367.

Appendix A: Pionless EFT for nucleons and baryons

In this appendix, we introduce the pionless EFT, which is essentially a non-relativistic quantum field theory for fermions. The goal is to explain how to reproduce ERE in Eq. (13) in an EFT and discuss the power counting scheme for unnaturally large scattering length.

In a non-relativistic EFT, the scaling of t differs from that of \vec{x} [27]:¹³

$$\vec{x} \rightarrow \lambda \vec{x}, \quad \frac{t}{M} \rightarrow \lambda^2 \frac{t}{M}, \quad \psi \rightarrow \lambda^{-3/2} \psi, \quad (\text{A1})$$

which leaves the kinetic terms in Eq. (16) invariant. The scaling makes it transparent that the Wilson coefficient of an operator with $2n$ spatial derivatives, C_{2n} , is of order

$$C_{2n} \sim \mathcal{O}\left(\frac{1}{M\Lambda^{2n+1}}\right). \quad (\text{A2})$$

In this power counting scheme, the leading order diagram is the tree-level diagram with the

¹³ To understand the scaling of t , recall the non-relativistic dispersion $E = |\vec{p}|^2/(2M)$.

C_0 vertex, as can be seen from Fig. 1:

$$\mathcal{A}_0 = -C_0 . \quad (\text{A3})$$

It reproduces Eq. (14) if

$$C_0 = \frac{4\pi a}{M} . \quad (\text{A4})$$

Going to higher orders in Fig. 1 we need to evaluate UV divergent loop integrals, in D spacetime dimensions, of the form [17, 18]

$$\begin{aligned} I_n &= -i(\mu/2)^{4-D} \int \frac{d^D q}{(2\pi)^D} \frac{i^2 \mathbf{q}^{2n}}{(E/2 + q_0 - \mathbf{q}^2/2M + i\epsilon)(E/2 - q_0 - \mathbf{q}^2/2M + i\epsilon)} \\ &= -\frac{(\mu/2)^{4-D}}{(4\pi)^{(D-1)/2}} \Gamma\left(\frac{3-D}{2}\right) M(ME)^n (-ME - i\epsilon)^{(D-3)/2} , \end{aligned} \quad (\text{A5})$$

and a subtraction scheme is needed. Recall the ERE in the denominator of Eq. (12) is a polynomial in p , which the EFT aims to reproduce. A subtraction scheme that achieves this goal is the minimal subtraction (MS) which removes the $1/(D-4)$ divergence, if any, and leads to [28]

$$I_n^{MS} = (ME)^n \left(\frac{M}{4\pi}\right) \sqrt{-ME - i\epsilon} = -i \left(\frac{M}{4\pi}\right) p^{2n+1} . \quad (\text{A6})$$

The nice feature that the loop momentum \mathbf{q} in I_n^{MS} gets converted to the external momentum p allows one to use the tree-level, on-shell vertex at the operator insertion in the loop diagram. Evaluating the loop diagrams in Fig. 1 and comparing with Eq. (14) order by order in p^n we arrive at the following relations in the MS scheme [17, 18]:

$$\mathcal{A}_0 = -C_0 , \quad \mathcal{A}_1 = i \frac{C_0^2 M p}{4\pi} , \quad \mathcal{A}_2 = \frac{C_0^3 M^2 p^2}{16\pi^2} - C_2 p^2 , \quad (\text{A7})$$

which give

$$C_0 = \frac{4\pi a}{M} , \quad C_2 = C_0 \frac{a r_0}{2} . \quad (\text{A8})$$

Notice that in the MS scheme C_{2n} is independent of the renormalization scale μ . Also in this scheme, if $|a| \lesssim 1/\Lambda$, the perturbative expansion converges up to Λ and the power counting in Eq. (A2) is reproduced. The EFT in this case could describe a bound state well below the threshold.

On the other hand, if $a \gg 1/\Lambda \sim 1/m_\pi$, Eq. (A4) is incompatible with the naive expecta-

$$\begin{aligned}
\mathcal{A}_{-1} &= \text{[Tree-level diagram with solid black vertex]} + \text{[One-loop bubble diagram with solid black vertices]} + \text{[Two-loop bubble diagram with solid black vertices]} + \dots \\
&\quad -C_0 \qquad C_0^2 \frac{M(\mu+ip)}{4\pi} \qquad -C_0^3 \left(\frac{M(\mu+ip)}{4\pi}\right)^2 \\
\mathcal{A}_0 &= \text{[Tree-level diagram with grey vertex]} + \text{[One-loop bubble diagram with grey vertices]} + \text{[Two-loop bubble diagram with grey vertices]} + \dots \\
&\quad -C_2 p^2 \qquad C_2 p^2 \frac{C_0 M(\mu+ip)}{4\pi} \qquad -C_2 p^2 \left(\frac{C_0 M(\mu+ip)}{4\pi}\right)^2
\end{aligned}$$

FIG. 3. The diagrams contributing to leading order s -wave amplitudes \mathcal{A}_{-1} and \mathcal{A}_0 in the center-of-mass frame under PDS scheme. A solid black vertex represents the $-C_0$ vertex, and a grey vertex represents the $-C_2 p^2$ vertex.

tion $C_0 \sim 1/(M\Lambda)$ and the perturbative expansion in C_0 would not converge in the regime $|1/a| \lesssim p \lesssim \Lambda$. The physics behind the breakdown of perturbative expansion in the case of large scattering lengths is the presence of shallow bound states, which manifest themselves as poles in the amplitudes. In this case, one needs to reproduce a different amplitude expansion from ERE, Eq. (15). The leading order term in eq. (15) scales as p^{-1} , and since every diagram has a positive order of p , \mathcal{A}_{-1} in eq. (15) has to come from an infinite sum of diagrams. As pointed out by Weinberg [20, 21], poles can be generated by resumming the bubble diagrams (see Fig. 1) with any number of C_0 insertions:

$$\begin{aligned}
\mathcal{A}^{resum} &= -\frac{C_0}{M} + \left(-\frac{C_0}{M}\right) I_0 \left(-\frac{C_0}{M}\right) + \left(-\frac{C_0}{M}\right) I_0 \left(-\frac{C_0}{M}\right) I_0 \left(-\frac{C_0}{M}\right) + \dots \\
&= \frac{1}{(C_0/M)^{-1} - I_0}. \tag{A9}
\end{aligned}$$

Resumming the bubble diagrams is equivalent to solving the Schrödinger equation with the potential given by C_0 . [20, 21].

To reproduce eq. (15) in the EFT, one could use a different subtraction scheme, the PDS scheme, and resum all bubble diagrams with insertions of C_0 , as shown in Fig. 3. This is what is known as the KSW-vK scheme. [17, 18, 22, 28–30]. Under PDS scheme, the

$1/(D - 3)$ divergence is also removed,

$$\delta I_n = -\frac{M(ME)^n \mu}{4\pi(D - 3)}, \quad I_n^{PDS} = -\frac{\mu + ip}{4\pi} M(ME)^n = \frac{-M(\mu + ip)p^{2n}}{4\pi}. \quad (\text{A10})$$

The resummed amplitude under PDS scheme is

$$\mathcal{A}^{resum,PDS} = -\frac{\sum_n C_{2n} p^{2n}}{1 + M(\mu + ip)/4\pi \sum_n C_{2n} p^{2n}}. \quad (\text{A11})$$

To match it to ERE, we consider the quantity

$$p \cot \delta = \frac{4\pi}{M\mathcal{A}} + ip = -\frac{4\pi}{M \sum_n C_{2n} p^{2n}} - \mu. \quad (\text{A12})$$

Comparing the Taylor expansion of eq. (A12) and eq. 13, we get

$$C_0 = \frac{4\pi}{M(1/a - \mu)}, \quad C_2 = \frac{r_0}{2} \frac{C_0}{1/a - \mu}. \quad (\text{A13})$$

The leading order terms in amplitude expansion are

$$\mathcal{A}_{-1} = \frac{-C_0}{1 + \frac{C_0 M}{4\pi}(\mu + ip)}, \quad \mathcal{A}_0 = \frac{-C_2 p^2}{\left[1 + \frac{C_0 M}{4\pi}(\mu + ip)\right]^2}. \quad (\text{A14})$$

It is now evident that \mathcal{A}_{-1} comprises diagrams with the vertex C_0 to all orders, and \mathcal{A}_0 comprises diagrams with one C_2 insertion and C_0 insertions to all orders. The MS scheme results can be recovered by setting $\mu = 0$.

Appendix B: Baryon-baryon scattering channels

The $SU(2)_{spin} \times SU(3)_{flavor}$ symmetry dictates low-energy baryon-baryon interactions. The lowest lying baryons have spin $1/2$ and transform as an eight-dimensional adjoint representation under $SU(3)$ flavor symmetry. Just as two $1/2$ spins can be projected into total spin $S = 0$ and $S = 1$ states, the 64-dimensional two-baryon flavor space is divided into six irreducible representations (irreps) of $SU(3)$, according to $\mathbf{8} \otimes \mathbf{8} = \mathbf{27} \oplus \mathbf{10} \oplus \overline{\mathbf{10}} \oplus \mathbf{8}_S \oplus \mathbf{8}_A \oplus \mathbf{1}$. We list the states of each irrep in the flavor eigenbasis in Tables VII-XII, which are then used to determine projection matrices in each flavor sector. It is important to keep in mind

that flavors of the two baryons are symmetrized in $\{\mathbf{27}, \mathbf{8}_S, \mathbf{1}\}$ irreps and anti-symmetrized in $\{\mathbf{10}, \overline{\mathbf{10}}, \mathbf{8}_A\}$ irreps, as we omit symmetric/antisymmetric subscripts in the tables for simplicity.

We briefly outline the computation process below. Since the Lagrangian is $SU(3)$ invariant, the tensor product decomposition dictates that the Lagrangian is a sum of six $SU(3)$ -symmetric operators which mediate 2-to-2 scattering for each of the irreps separately, and whose coefficient will be denoted as $\{C_{\mathbf{27}}, C_{\mathbf{10}}, C_{\overline{\mathbf{10}}}, C_{\mathbf{8}_S}, C_{\mathbf{8}_A}, C_{\mathbf{1}}\}$. The $SU(3)$ symmetry further determines that each operator has to be diagonal in the $SU(3)$ -symmetric basis. Since Q and S are conserved, the Lagrangian can also be split into different (Q, S) sectors,

$$\mathcal{L} = \sum_{Q,S} \mathcal{L}_{Q,S} . \quad (\text{B1})$$

Each $\mathcal{L}_{Q,S}$ contains channels from different irreps. One can compute $\mathcal{L}_{Q,S}$ by expanding Eq. (23) in terms of individual baryon fields and picking out terms in desired (Q, S) sector. $\mathcal{L}_{Q,S}$ is then organized into the diagonal form. For example, the Lagrangian involving the $\{\Sigma^0 n, \Sigma^- p, \Lambda n\}$ sector is diagonalized as

$$\begin{aligned} \mathcal{L}_{Q=0,S=-1} = & -(c_1 - c_2 + c_5 - c_6)(\psi_1^\dagger \psi_1 + \psi_2^\dagger \psi_2) \\ & - \left(-\frac{2}{3}c_1 + \frac{2}{3}c_2 - \frac{5}{6}c_3 + \frac{5}{6}c_4 + c_5 - c_6 \right) \psi_3^\dagger \psi_3 \\ & - (c_1 + c_2 + c_5 + c_6) (\psi_4^{(1)\dagger} \psi_4^{(1)} + \psi_4^{(2)\dagger} \psi_4^{(2)} + \psi_4^{(3)\dagger} \psi_4^{(3)}) \\ & - (-c_1 - c_2 + c_5 + c_6) (\psi_5^{(1)\dagger} \psi_5^{(1)} + \psi_5^{(2)\dagger} \psi_5^{(2)} + \psi_5^{(3)\dagger} \psi_5^{(3)}) \\ & - \left(\frac{3}{2}c_3 + \frac{3}{2}c_4 + c_5 + c_6 \right) (\psi_6^{(1)\dagger} \psi_6^{(1)} + \psi_6^{(2)\dagger} \psi_6^{(2)} + \psi_6^{(3)\dagger} \psi_6^{(3)}) , \end{aligned} \quad (\text{B2})$$

where

$$\psi_1 = \sqrt{\frac{2}{3}} \left(\frac{\Sigma_\uparrow^0 n_\downarrow - \Sigma_\downarrow^0 n_\uparrow}{\sqrt{2}} \right) + \sqrt{\frac{1}{3}} \left(\frac{\Sigma_\uparrow^- p_\downarrow - \Sigma_\downarrow^- p_\uparrow}{\sqrt{2}} \right) , \quad (\text{B3})$$

$$\psi_2 = -\sqrt{\frac{1}{30}} \left(\frac{\Sigma_\uparrow^0 n_\downarrow - \Sigma_\downarrow^0 n_\uparrow}{\sqrt{2}} \right) + \sqrt{\frac{1}{15}} \left(\frac{\Sigma_\uparrow^- p_\downarrow - \Sigma_\downarrow^- p_\uparrow}{\sqrt{2}} \right) + \sqrt{\frac{9}{10}} \left(\frac{\Lambda_\uparrow n_\downarrow - \Lambda_\downarrow n_\uparrow}{\sqrt{2}} \right) , \quad (\text{B4})$$

$$\psi_3 = \sqrt{\frac{3}{10}} \left(\frac{\Sigma_\uparrow^0 n_\downarrow - \Sigma_\downarrow^0 n_\uparrow}{\sqrt{2}} \right) - \sqrt{\frac{3}{5}} \left(\frac{\Sigma_\uparrow^- p_\downarrow - \Sigma_\downarrow^- p_\uparrow}{\sqrt{2}} \right) + \sqrt{\frac{1}{10}} \left(\frac{\Lambda_\uparrow n_\downarrow - \Lambda_\downarrow n_\uparrow}{\sqrt{2}} \right) , \quad (\text{B5})$$

$$\psi_4^{(1)} = \sqrt{\frac{2}{3}} \Sigma_{\uparrow}^0 n_{\uparrow} + \sqrt{\frac{1}{3}} \Sigma_{\uparrow}^- p_{\uparrow} , \quad (\text{B6})$$

$$\psi_5^{(1)} = -\sqrt{\frac{1}{6}} \Sigma_{\uparrow}^0 n_{\uparrow} + \sqrt{\frac{1}{3}} \Sigma_{\uparrow}^- p_{\uparrow} + \sqrt{\frac{1}{2}} \Lambda_{\uparrow} n_{\uparrow} , \quad (\text{B7})$$

$$\psi_6^{(1)} = -\sqrt{\frac{1}{6}} \Sigma_{\uparrow}^0 n_{\uparrow} + \sqrt{\frac{1}{3}} \Sigma_{\uparrow}^- p_{\uparrow} - \sqrt{\frac{1}{2}} \Lambda_{\uparrow} n_{\uparrow} . \quad (\text{B8})$$

By replacing operators $F_{1\uparrow}F_{2\uparrow}$ in $\psi_i^{(1)}$ with $(F_{1\uparrow}F_{2\downarrow} + F_{1\downarrow}F_{2\uparrow})/\sqrt{2}$ or $F_{1\downarrow}F_{2\downarrow}$, one gets $\psi_i^{(2)}$ or $\psi_i^{(3)}$. Scattering channels can be read off and are listed in Eqs. (38)-(43). To further identify the irrep of each ψ_i , we compute the eigenvalues of Casimir operators acting on these states. $SU(3)$ has two Casimir operators,

$$\mathcal{C}_1 = \sum_a T^a T^a , \quad \mathcal{C}_2 = \sum_{abc} d^{abc} T^a T^b T^c , \quad (\text{B9})$$

where $d^{abc} = 2\text{Tr}(\{T^a, T^b\}T^c)$ is the totally symmetric d constants of $SU(3)$. Here $\mathcal{C}_1 = (p^2 + q^2 + 3p + 3q + pq)/3$ and $\mathcal{C}_2 = (p - q)(3 + p + 2q)(3 + q + 2p)/18$, where (p, q) for the irreps are: $\mathbf{27} = (2, 2)$, $\mathbf{10} = (3, 0)$, $\overline{\mathbf{10}} = (0, 3)$, $\mathbf{8} = (\mathbf{1}, \mathbf{1})$, and $\mathbf{1} = (\mathbf{0}, \mathbf{0})$ [31]. Every irrep can be determined by a unique set of eigenvalues of \mathcal{C}_1 and \mathcal{C}_2 . This process also allows us to find the values of $C_{\mathbf{27}}, C_{\mathbf{10}}, C_{\overline{\mathbf{10}}}, C_{\mathbf{8}_S}$ and $C_{\mathbf{8}_A}$ in terms of the c_i . We complete the tables below by repeating this process for every (Q, S) sector. Alternatively, the states can be found using lowering operators in $SU(3)$. Since these states are weights of each irrep, one can start by identifying the unique highest weight in each irrep, whose (Q, S) values are fixed by the representation theory. To find the highest weights of $\mathbf{8}_S, \mathbf{8}_A$ and $\mathbf{1}$, it is useful to also consider the action of two Casimir operators, which fixes the linear combination of multiple physical states with same (Q, S) values. Then one can derive all remaining weights by repeated action of three lowering operators, $I_- = T^1 - iT^2, V_- = T^4 - iT^5$, and $U_- = T^6 - iT^7$.

scattering channels
nn
np
pp
$n\Sigma^-$
$\sqrt{\frac{2}{3}}\Sigma^0 n + \sqrt{\frac{1}{3}}\Sigma^- p$
$-\sqrt{\frac{1}{30}}\Sigma^0 n + \sqrt{\frac{1}{15}}\Sigma^- p + \sqrt{\frac{9}{10}}\Lambda n$
$-\sqrt{\frac{1}{3}}\Sigma^+ n + \sqrt{\frac{2}{3}}\Sigma^0 p$
$\sqrt{\frac{1}{15}}\Sigma^+ n + \sqrt{\frac{1}{30}}\Sigma^0 p + \sqrt{\frac{9}{10}}\Lambda p$
$\Sigma^+ p$
$\sqrt{\frac{1}{3}}\Sigma^+ \Sigma^- - \sqrt{\frac{2}{3}}\Sigma^0 \Sigma^0$
$\sqrt{\frac{3}{5}}\Lambda \Sigma^0 + \sqrt{\frac{1}{5}}\Xi^- p - \sqrt{\frac{1}{5}}\Xi^0 n$
$\sqrt{\frac{1}{60}}\Sigma^+ \Sigma^- - \sqrt{\frac{1}{120}}\Sigma^0 \Sigma^0 - \sqrt{\frac{3}{20}}\Xi^0 n - \sqrt{\frac{3}{20}}\Xi^- p + \sqrt{\frac{27}{40}}\Lambda \Lambda$
$\Sigma^- \Sigma^-$
$\Sigma^- \Sigma^0$
$\sqrt{\frac{3}{5}}\Lambda \Sigma^- - \sqrt{\frac{2}{5}}\Xi^- n$
$\sqrt{\frac{3}{5}}\Lambda \Sigma^+ - \sqrt{\frac{2}{5}}\Xi^0 p$
$\Sigma^+ \Sigma^0$
$\Sigma^+ \Sigma^+$
$\Sigma^- \Xi^-$
$-\sqrt{\frac{2}{3}}\Sigma^0 \Xi^- + \sqrt{\frac{1}{3}}\Sigma^- \Xi^0$
$-\sqrt{\frac{1}{30}}\Sigma^0 \Xi^- + \sqrt{\frac{1}{15}}\Sigma^- \Xi^0 + \sqrt{\frac{9}{10}}\Lambda \Xi^-$
$\sqrt{\frac{1}{3}}\Sigma^+ \Xi^- + \sqrt{\frac{2}{3}}\Sigma^0 \Xi^0$
$-\sqrt{\frac{1}{15}}\Sigma^+ \Xi^- + \sqrt{\frac{1}{30}}\Sigma^0 \Xi^0 + \sqrt{\frac{9}{10}}\Lambda \Xi^0$
$\Sigma^+ \Xi^0$
$\Xi^- \Xi^-$
$\Xi^- \Xi^0$
$\Xi^0 \Xi^0$

TABLE VII. Baryon-baryon scattering channels in **27**.

scattering channels
$\sqrt{\frac{3}{10}}\Sigma^0 n - \sqrt{\frac{3}{5}}\Sigma^- p + \sqrt{\frac{1}{10}}\Lambda n$
$\sqrt{\frac{3}{5}}\Sigma^+ n + \sqrt{\frac{3}{10}}\Sigma^0 p - \sqrt{\frac{1}{10}}\Lambda p$
$-\sqrt{\frac{2}{5}}\Lambda\Sigma^0 + \sqrt{\frac{3}{10}}\Xi^- p - \sqrt{\frac{3}{10}}\Xi^0 n$
$\sqrt{\frac{2}{5}}\Sigma^+\Sigma^- - \sqrt{\frac{1}{5}}\Sigma^0\Sigma^0 + \sqrt{\frac{1}{10}}\Xi^0 n + \sqrt{\frac{1}{10}}\Xi^- p + \sqrt{\frac{1}{5}}\Lambda\Lambda$
$\sqrt{\frac{2}{5}}\Lambda\Sigma^- + \sqrt{\frac{3}{5}}\Xi^- n$
$\sqrt{\frac{2}{5}}\Lambda\Sigma^+ + \sqrt{\frac{3}{5}}\Xi^0 p$
$\sqrt{\frac{3}{10}}\Sigma^0\Xi^- + \sqrt{\frac{3}{5}}\Sigma^-\Xi^0 - \sqrt{\frac{1}{10}}\Lambda\Xi^-$
$\sqrt{\frac{3}{5}}\Sigma^+\Xi^- - \sqrt{\frac{3}{10}}\Sigma^0\Xi^0 + \sqrt{\frac{1}{10}}\Lambda\Xi^0$

TABLE VIII. Baryon-baryon scattering channels in $\mathbf{8}_S$.

scattering channels
$\frac{1}{2}\Sigma^+\Sigma^- + \sqrt{\frac{1}{8}}\Sigma^0\Sigma^0 + \frac{1}{2}\Xi^0 n + \frac{1}{2}\Xi^- p + \sqrt{\frac{1}{8}}\Lambda\Lambda$

TABLE IX. Baryon-baryon scattering channels in $\mathbf{1}$.

scattering channels
np
$-\sqrt{\frac{1}{6}}\Sigma^0 n + \sqrt{\frac{1}{2}}\Sigma^- p + \sqrt{\frac{1}{2}}\Lambda n$
$\sqrt{\frac{1}{3}}\Sigma^+ n + \sqrt{\frac{1}{6}}\Sigma^0 p - \sqrt{\frac{1}{2}}\Lambda p$
$\sqrt{\frac{1}{2}}\Lambda\Sigma^- - \sqrt{\frac{1}{6}}\Sigma^-\Sigma^0 - \sqrt{\frac{1}{3}}\Xi^- n$
$\sqrt{\frac{1}{2}}\Lambda\Sigma^+ - \sqrt{\frac{1}{6}}\Sigma^+\Sigma^0 - \sqrt{\frac{1}{3}}\Xi^0 p$
$\Sigma^-\Xi^-$
$-\sqrt{\frac{2}{3}}\Sigma^0\Xi^- + \sqrt{\frac{1}{3}}\Sigma^-\Xi^0$
$\sqrt{\frac{1}{3}}\Sigma^+\Xi^- + \sqrt{\frac{2}{3}}\Sigma^0\Xi^0$
$\Sigma^+\Xi^0$

TABLE X. Baryon-baryon scattering channels in $\overline{\mathbf{10}}$.

scattering channels
$n\Sigma^-$
$\sqrt{\frac{2}{3}}\Sigma^0 n + \sqrt{\frac{1}{3}}\Sigma^- p$
$-\sqrt{\frac{1}{3}}\Sigma^+ n + \sqrt{\frac{2}{3}}\Sigma^0 p$
$\Sigma^+ p$
$\sqrt{\frac{1}{2}}\Lambda\Sigma^- + \sqrt{\frac{1}{6}}\Sigma^-\Sigma^0 + \sqrt{\frac{1}{3}}\Xi^- n$
$\sqrt{\frac{1}{2}}\Lambda\Sigma^+ + \sqrt{\frac{1}{6}}\Sigma^+\Sigma^0 + \sqrt{\frac{1}{3}}\Xi^0 p$
$-\sqrt{\frac{1}{6}}\Sigma^0\Xi^- + \sqrt{\frac{1}{3}}\Sigma^-\Xi^0 - \sqrt{\frac{1}{2}}\Lambda\Xi^-$
$-\sqrt{\frac{1}{3}}\Sigma^+\Xi^- + \sqrt{\frac{1}{6}}\Sigma^0\Xi^0 + \sqrt{\frac{1}{2}}\Lambda\Xi^0$
$\Xi^-\Xi^0$

TABLE XI. Baryon-baryon scattering channels in **10**.

scattering channels
$-\sqrt{\frac{1}{6}}\Sigma^0 n + \sqrt{\frac{1}{2}}\Sigma^- p + \sqrt{\frac{1}{2}}\Lambda n$
$\sqrt{\frac{1}{3}}\Sigma^+ n + \sqrt{\frac{1}{6}}\Sigma^0 p - \sqrt{\frac{1}{2}}\Lambda p$
$-\sqrt{\frac{2}{3}}\Sigma^-\Sigma^0 + \sqrt{\frac{1}{3}}\Xi^- n$
$\sqrt{\frac{1}{2}}\Xi^0 n + \sqrt{\frac{1}{2}}\Xi^- p$
$-\sqrt{\frac{1}{6}}\Xi^0 n + \sqrt{\frac{1}{6}}\Xi^- p + \sqrt{\frac{2}{3}}\Sigma^-\Sigma^+$
$-\sqrt{\frac{2}{3}}\Sigma^+\Sigma^0 + \sqrt{\frac{1}{3}}\Xi^0 p$
$-\sqrt{\frac{1}{6}}\Sigma^0\Xi^- + \sqrt{\frac{1}{3}}\Sigma^-\Xi^0 + \sqrt{\frac{1}{2}}\Lambda\Xi^-$
$-\sqrt{\frac{1}{3}}\Sigma^+\Xi^- + \sqrt{\frac{1}{6}}\Sigma^0\Xi^0 - \sqrt{\frac{1}{2}}\Lambda\Xi^0$

TABLE XII. Baryon-baryon scattering channels in **8_A**.

-
- [1] S. R. Beane, D. B. Kaplan, N. Klco, and M. J. Savage, Phys. Rev. Lett. **122**, 102001 (2019), arXiv:1812.03138 [nucl-th].
- [2] I. Low and T. Mehen, Phys. Rev. D **104**, 074014 (2021), arXiv:2104.10835 [hep-th].
- [3] E. Wigner, Phys. Rev. **51**, 106 (1937).
- [4] T. Mehen, I. W. Stewart, and M. B. Wise, Phys. Rev. Lett. **83**, 931 (1999), arXiv:hep-ph/9902370.
- [5] T. Mehen, I. W. Stewart, and M. B. Wise, Phys. Lett. B **474**, 145 (2000), arXiv:hep-th/9910025.
- [6] M. L. Wagman, F. Winter, E. Chang, Z. Davoudi, W. Detmold, K. Orginos, M. J. Savage, and P. E. Shanahan, Phys. Rev. D **96**, 114510 (2017), arXiv:1706.06550 [hep-lat].
- [7] D. B. Kaplan and M. J. Savage, Phys. Lett. B **365**, 244 (1996), arXiv:hep-ph/9509371.
- [8] M. J. Savage and M. B. Wise, Phys. Rev. D **53**, 349 (1996), arXiv:hep-ph/9507288.
- [9] R. Aoude, M.-Z. Chung, Y.-t. Huang, C. S. Machado, and M.-K. Tam, Phys. Rev. Lett. **125**, 181602 (2020), arXiv:2007.09486 [hep-th].
- [10] B.-T. Chen, M.-Z. Chung, Y.-t. Huang, and M. K. Tam, JHEP **10**, 011 (2021), arXiv:2106.12518 [hep-th].
- [11] S. R. Beane, R. C. Farrell, and M. Varma, Int. J. Mod. Phys. A **36**, 2150205 (2021), arXiv:2108.00646 [hep-ph].
- [12] A. Cervera-Lierta, J. I. Latorre, J. Rojo, and L. Rottoli, SciPost Phys. **3**, 036 (2017), arXiv:1703.02989 [hep-th].
- [13] P. Zanardi, Phys. Rev. A **63**, 040304 (2001).
- [14] A. D. Ballard and Y.-S. Wu, in *Cross disciplinary advances in quantum computing* (American Mathematical Society, Oxford, 2011) Chap. Cartan Decomposition and Entangling Power of Braiding Quantum Gates.
- [15] M. L. Goldberger and K. M. Watson, *Collision Theory* (Wiley, New York, 1964).
- [16] H. A. Bethe, Phys. Rev. **76**, 38 (1949).
- [17] D. B. Kaplan, M. J. Savage, and M. B. Wise, Phys. Lett. B **424**, 390 (1998), arXiv:nucl-th/9801034.
- [18] D. B. Kaplan, M. J. Savage, and M. B. Wise, Nucl. Phys. B **534**, 329 (1998), arXiv:nucl-

th/9802075.

- [19] U. van Kolck, Eur. Phys. J. A **56**, 97 (2020), arXiv:2003.09974 [nucl-th].
- [20] S. Weinberg, Phys. Lett. B **251**, 288 (1990).
- [21] S. Weinberg, Nucl. Phys. B **363**, 3 (1991).
- [22] U. van Kolck, Nucl. Phys. A **645**, 273 (1999), arXiv:nucl-th/9808007.
- [23] Q. Liu, “Entanglement in low energy qcd,” Undergraduate thesis, Duke University, unpublished.
- [24] M. Gell-Mann, Phys. Rev. **125**, 1067 (1962).
- [25] M. Illa *et al.* (NPLQCD), Phys. Rev. D **103**, 054508 (2021), arXiv:2009.12357 [hep-lat].
- [26] A. Cervera-Lierta, J. I. Latorre, J. Rojo, and L. Rottoli, SciPost Phys. **3**, 036 (2017), arXiv:1703.02989 [hep-th].
- [27] C. R. Hagen, Phys. Rev. D **5**, 377 (1972).
- [28] D. B. Kaplan (2005) arXiv:nucl-th/0510023.
- [29] P. F. Bedaque and U. van Kolck, Phys. Lett. B **428**, 221 (1998), arXiv:nucl-th/9710073.
- [30] U. van Kolck, Lect. Notes Phys. **513**, 62 (1998), arXiv:hep-ph/9711222.
- [31] H. Georgi, *Lie Algebras In Particle Physics : from Isospin To Unified Theories* (Taylor & Francis, Boca Raton, 2000).